NATIONAL ENERGY TECHNOLOGY LABORATORY

OPERATION OF THE NETL CHEMICAL LOOPING REACTOR WITH NATURAL GAS AND A NOVEL COPPER-IRON MATERIAL

February, **2017**

NETL-PUB-20912

U.S. DEPARTMENT OF ENERGY | NATIONAL ENERGY TECHNOLOGY LABORATORY

DISCLAIMER

Cover Illustration: The 50-kWth natural gas Chemical Looping Reactor (CLR) at the National Energy Technology Laboratory's Morgantown, WV facility.

Suggested Citation: Bayham, S., Straub, D., and Weber, J., "Operation of the NETL Chemical Looping Reactor with Natural Gas and a Novel Copper-Iron Material," NETL-PUB-20912; NETL Technical Report Series; U.S. Department of Energy, National Energy Technology Laboratory: Morgantown, WV, 2017

An electronic version of this report has been uploaded to the Office of Science, Technology, and Industry website at: http://www.osti.gov/bridge.

Operation of the NETL Chemical Looping Reactor with Natural Gas and a Novel Copper-Iron Material

Samuel Bayham, Doug Straub, and Justin Weber

Research and Innovation Center, National Energy Technology Laboratory, Morgantown, WV 26507

NETL-PUB-20912

February 2017

NETL Contacts:

Samuel Bayham, Principal Investigator

Doug Straub, Technical Portfolio Lead

Geo Richards, Senior Research Fellow

This page intentionally left blank.

Table of Contents

List of Figures

List of Tables

Acronyms, Abbreviations, and Symbols

Symbol	Definition (units)
A_i	Cross sectional area of bed *i* (m^2)
a, b	Fitting parameters for circulation rate equation from riser crossover pressure drop
C_{bal}	Carbon balance term (ratio of carbon atoms out divided by carbon atoms in) (-)
f_i	Weight fraction of species *i* in oxygen carrier (kg/kg)
g	Acceleration of gravity (9.81 m/s^2)
$HHV_{\mathrm{CH_4}}$	Higher heating value of methane (kJ/mol)
$h_{\mathrm{bed},i}$	Height of bed *i* (m)
m_{added}	Mass of solids added to system (kg)
$m_{\mathrm{bed},i}$	Solids inventory in reactor *i* (kg)
m_{inv}	Estimated inventory of solids in system (kg)
m_{missing}	Calculated mass of solids missing from solids mass closure (kg)
$m_{\mathrm{out},i}$	Accumulated mass of solids collected from reactor *i* (kg)
$\dot{m}_{\mathrm{loss}}$	Rate of solids mass loss from the system (kg/h)
$\dot{m}_{\mathrm{OC}}$	Solids circulation rate (kg/h)
MW_i	Molecular weight of species *i* (kg/mol)
$\dot{N}_{\mathrm{T,out}}$	Total molar flow rate of the flue gas (mol/h)
$\dot{N}_{i,\mathrm{in}}$	Molar flowrate of species *i* into the reactor (mol/h)
$\dot{N}_{i,\mathrm{out}}$	Molar flowrate of species *i* in the flue gas (mol/h)
$\dot{N}_{\mathrm{O,out}}$	Molar flowrate of atomic oxygen out of the fuel reactor (mol/h)
$\dot{N}_{\mathrm{O,total}}$	Total molar oxygen flow rate contained in the solid (mol/h)
P_i	Absolute pressure of reactor *i* (Pa)
ΔP_i	Pressure drop of reactor *i* (psid or Pa)
$Q^*_{\mathrm{N_2},\mathrm{in}}$	Total standard nitrogen volumetric flow rate (SCFH)
Q_{LM}	Log-mean average volumetric flow rate (SCFH)
$Q^*_{\mathrm{T,dry}}$	Total dry volumetric flow rate (SCFH)
$Q^*_{\mathrm{T,wet}}$	Total standard volumetric flow rate on a wet basis (SCFH)
$Q_{\mathrm{T,wet}}$	Total volumetric flow rate on a wet basis (SCFH)
Q_{in}	Volumetric flow rate in (SCFH)
R	Ideal gas law constant (L-atm/mol-K or J/mol-K)
t	Time (s)
T_i	Temperature of reactor *i* (°C)
$U_{\mathrm{g,LM}}$	Log-mean averaged gas velocity (m/s)
W_{OC}	Cost of oxygen carrier (US$/kg)
x_i	Coded independent parameters for regression analysis
$X_{\mathrm{CH_4}}$	Methane conversion (%)

$X_{\mathrm{CH_4 \rightarrow CO_2}}$	Methane conversion to carbon dioxide (%)
X_{OC}	Oxygen carrier conversion or utilization (mol/mol, %)
$y_{i,\mathrm{out,dry}}$	Mole fraction of species *i* in flue gas on a dry basis
$y_{i,\mathrm{out}}$	Mole fraction of species *i* in the flue gas on a wet basis
α	Fraction of oxygen carrier recycled
$\hat{\beta}_i$	Fitting parameters for regression analysis
ρ_B	Bulk density of solid (kg/m^3)
$\rho_{i,\mathrm{STD}}$	Density of gaseous species *i* at standard temperature and pressure (kg/m^3)
$\tau_{\mathrm{g},i}$	Gas residence time in reactor *i* (s)
$\tau_{\mathrm{OC},i}$	Solids residence time (s)

Acknowledgments

This work was funded by the U.S. Department of Energy's Advanced Combustion Program. The support of Rich Dennis, Dan Driscoll, John Rockey, Steve Markovich, and Briggs White are greatly appreciated. Dr. Ranjani Siriwardane, Jarrett Riley, William Benincosa, and Dr. Hanjing Tian have also played a critical role in this effort as the research team that developed this oxygen carrier material. The authors would also like to acknowledge the hard work and dedication of the operational staff of Dave Reese, Jeff Riley, Mark Tucker, and Richard Eddy. And finally, the Activity Manager, Steve Carpenter, and the Senior Research Fellow, Geo Richards, have provided unwavering support through the highs and lows, and their leadership is greatly appreciated.

EXECUTIVE SUMMARY

The proposed Clean Power Plan requires CO_2 emission reductions of 30% by 2030 and further reductions are targeted by 2050[1]. The current strategies to achieve the 30% reduction targets do not include options for coal. However, the 2016 Annual Energy Outlook[2] suggests that coal will continue to provide more electricity than renewable sources for many regions of the country in 2035. Therefore, cost effective options to reduce greenhouse gas emissions from fossil fuel power plants are vital in order to achieve greenhouse gas reduction targets beyond 2030.

As part of the U.S. Department of Energy's Advanced Combustion Program, the National Energy Technology Laboratory's Research and Innovation Center (NETL R&IC) is investigating the feasibility of a novel combustion concept in which the GHG emissions can be significantly reduced. This concept involves burning fuel and air without mixing these two reactants. If this concept is technically feasible, then CO_2 emissions can be significantly reduced at a much lower cost than more conventional approaches. This indirect combustion concept has been called Chemical Looping Combustion (CLC) because an intermediate material (i.e., a metal-oxide) is continuously cycled to oxidize the fuel. This CLC concept is the focus of this research and will be described in more detail in the following sections.

The solid material that is used to transport oxygen is called an oxygen carrier material. The cost, durability, and performance of this material is a key issue for the CLC technology. Researchers at the NETL R&IC have developed an oxygen carrier material that consists of copper, iron, and alumina. This material has been tested extensively using lab scale instruments such as thermogravimetric analysis (TGA), scanning electron microscopy (SEM), mechanical attrition (ASTM D*5757*), and small fluidized bed reactor tests. This report will describe the results from a realistic, circulating, proof-of-concept test that was completed using NETL's 50kW_{th} circulating Chemical Looping Reactor (CLR) test facility. The test campaign started on July 10, 2016 and continued for 5 days and 10 hours. The results are summarized below, but more details can be found in the body of this report.

- 4 days and 8 hours of oxygen carrier circulation in the target temperature range,
- 40 hours of chemical looping combustion testing,
- Fuel reactor temperatures ranged from 760-815°C,
- Air reactor temperatures ranged from 840-915°C
- Fuel conversion from natural gas to CO_2 ranged from 50-80%
- Over 100 minutes of continuous operation was achieved with no gas preheat and no natural gas augmented heating. During this period,
    - The fuel reactor temperature ranged from 780-825°C
    - The air reactor temperature ranged from 930-960°C
    - The fuel to CO_2 conversion ranged from 50-65%

In summary, the NETL developed Cu/Fe/alumina oxygen carrier material enabled stable operation at relatively low solids inventory and low solids circulation rates compared to other natural oxygen carriers that have been tested in this test facility. Some oxygen carrier material was lost throughout the course of this test, and there was evidence to suggest that some particle attrition was happening due to classic "abrasion" mechanisms. The future development for this particular oxygen carrier material should focus on reducing the cost and improving the abrasion resistance of this material.

This test facility has focused on the use of natural gas fuel to demonstrate the feasibility of the CLC concept and evaluate the carrier performance in a realistic thermal and hydrodynamic environment. Although the fuel-to-CO_2 conversion of 50-80% needs to be improved, the test data provides some insight into approaches to improve the fuel-to-CO_2 conversion. The future directions for this test facility include:

- Investigating the effect of higher pressure operation
- Adding steam to the fluidization gas mixture to improve the fuel conversion
- Testing carbon monoxide and hydrogen fuels that react much faster than natural gas

1. INTRODUCTION

Greenhouse gas (GHG) emissions, largely carbon dioxide, need to be curtailed from stationary sources such as fossil-fuel power plants. Carbon dioxide emissions from electricity generation account for nearly one-third of the total CO_2 emissions in the United States[1]. In order to achieve the GHG reduction targets beyond 2030, cost effective options are needed to reduce greenhouse gas emissions from fossil fuel power plants.

As part of the U.S. Department of Energy's Advanced Combustion Program, the National Energy Technology Laboratory's Research and Innovation Center (NETL R&IC) is investigating the feasibility of novel combustion concepts in which GHG emissions can be significantly reduced. Conventional post-combustion CO_2 capture approaches must separate carbon dioxide from nitrogen and other gaseous species in a typical flue gas. The parasitic energy penalties associated with these types of gaseous separation technologies is significant. Therefore, if the novel combustion concepts being developed under DOE's Advanced Combustion Program are feasible alternatives, then alternatives can be developed to meet the GHG reduction targets for fossil fuel power plants in the future.

The alternative "combustion" process that will be discussed in this report is called Chemical Looping Combustion (CLC). The CLC concept is based on oxygen transport to the carbonaceous fuel using an intermediate material (i.e., metal oxide). These intermediate materials are called oxygen carrier materials and cost-effective CO_2 capture can be achieved by splitting the oxidation/reduction process into two separate stages, as shown in Figure 1. This process significantly reduces the energy penalty of carbon dioxide separation.

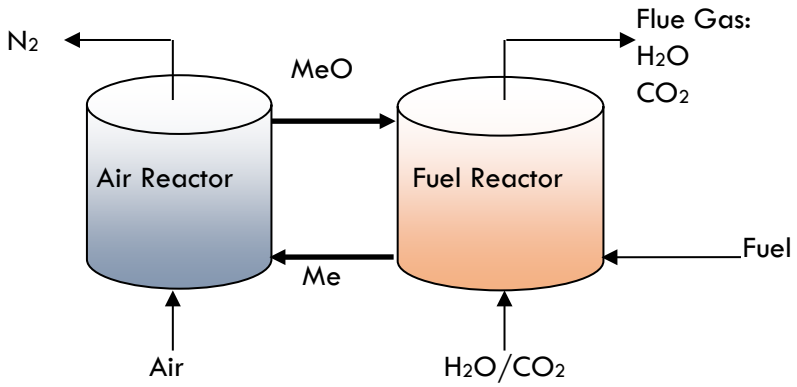

FIGURE 1. CHEMICAL LOOPING COMBUSTION CONCEPT.

The chemical looping combustion process was initially envisioned in 1954 as a method to produce pure carbon dioxide as an industrial process[3]. The CLC process is an attractive method to capture carbon dioxide because the combustion products never directly mix with the air used to oxidize the fuel. Since the 1990's, interest in chemical looping combustion for power generation applications has grown significantly[4]. In a recent study conducted at the National Energy Technology Laboratory[5], two CLC plant configurations were compared to a conventional coal power plant with a conventional downstream CO_2 capture technology. For both CLC configurations, the capital cost and subsequent cost of electricity was significantly lower than the conventional approach.

Although the recent developments and studies are encouraging, significant technical challenges must be addressed before this concept can become a commercially feasible option for fossil energy. Two of the largest challenges include 1) demonstrating key oxygen carrier performance characteristics (i.e., cost, reactivity, and durability), and 2) demonstrating reliable bulk solids handling. For example, depending on the oxygen carrier material that is selected, large circulation rates of solids between the air and fuel reactors

can be required. In some CLC configurations, the circulation rate of oxygen carrier material can be orders of magnitude higher than the fuel flow. Therefore, the ability to control and operate a CLC process can become a potential barrier issue.

For the first part of the problem, the NETL R&IC is developing a copper/iron/aluminum oxide oxygen carrier material that has shown promising results in laboratory-scale testing. This material has been tested at NETL using thermogravimetric analysis (TGA), scanning electron microscopy (SEM), small fluidized bed reaction cycling, and attrition resistance[6]. The second generation oxygen carrier material is very similar in many ways to the first generation. The second generation material has also demonstrated high oxygen transport capacity (>10 wt%), high oxygen carrier reactivity, and a neutral heat of reaction during the reduction stage. The primary difference between the first and the second generation materials is the manufacturing process. Instead of using a spray drying process, the second generation material has been fabricated using a wet granulation method. This method has the potential to significantly reduce the manufacturing cost which is critical for reducing projected operating costs of some CLC process configurations.

For the second (i.e., bulk solids handling) challenge, NETL has designed, constructed, and operated a fully integrated chemical looping reactor (CLR) test facility. This test facility has been designed for 50 kW_{th} natural gas and located at NETL's Morgantown, West Virginia site. Refractory lining has been incorporated throughout the system, and the test facility has been operated on natural gas. This test facility has been used to evaluate potential oxygen carrier materials in a realistic environment. Control schemes and performance benchmarks have also been investigated using this facility.

In July 2016, NETL's CLR facility operated over a one-week period to evaluate the performance of NETL's second generation copper-iron oxygen carrier. This report summarizes this first test campaign for NETL's second generation Cu/Fe/alumina oxygen carrier material. The report is organized as follows. The following section (Section 2) describes the experimental methods and procedures that were utilized during this test campaign. Section 3 describes the results from this test and provides a discussion of the key findings. Detailed results are also tabulated in the appendix of this report.

2. METHODS AND PROCEDURES

2.1 Test Rig Description

NETL's Chemical Looping Reactor is comprised of conventional refractory-lined carbon steel piping components. Since all of the carbon steel piping components are refractory lined, no external heat is added to the oxygen carrier flow path. This design feature is unique for CLC test facilities of this scale. As a result of this design approach, strategies for controlling the interconnected reactor temperatures in the presences of heat loss can be investigated.

A schematic of the NETL chemical looping system components and simplified process flow is shown in Figure 2. Some of the key system components in this test facility include a fuel reactor, an air reactor, and a seal pot. The seal pot prevents gas mixing between the other two reactors. The fuel reactor is currently configured as a bubbling fluidized bed reactor. The air reactor can be operated as a bubbling fluidized bed or a turbulent bed reactor depending on the air velocity. Both the fuel reactor and the seal pot have inner diameters of 8 inches. The air reactor has an inner diameter of 6 inches, and the riser section has an inner diameter of approximately 2 inches.

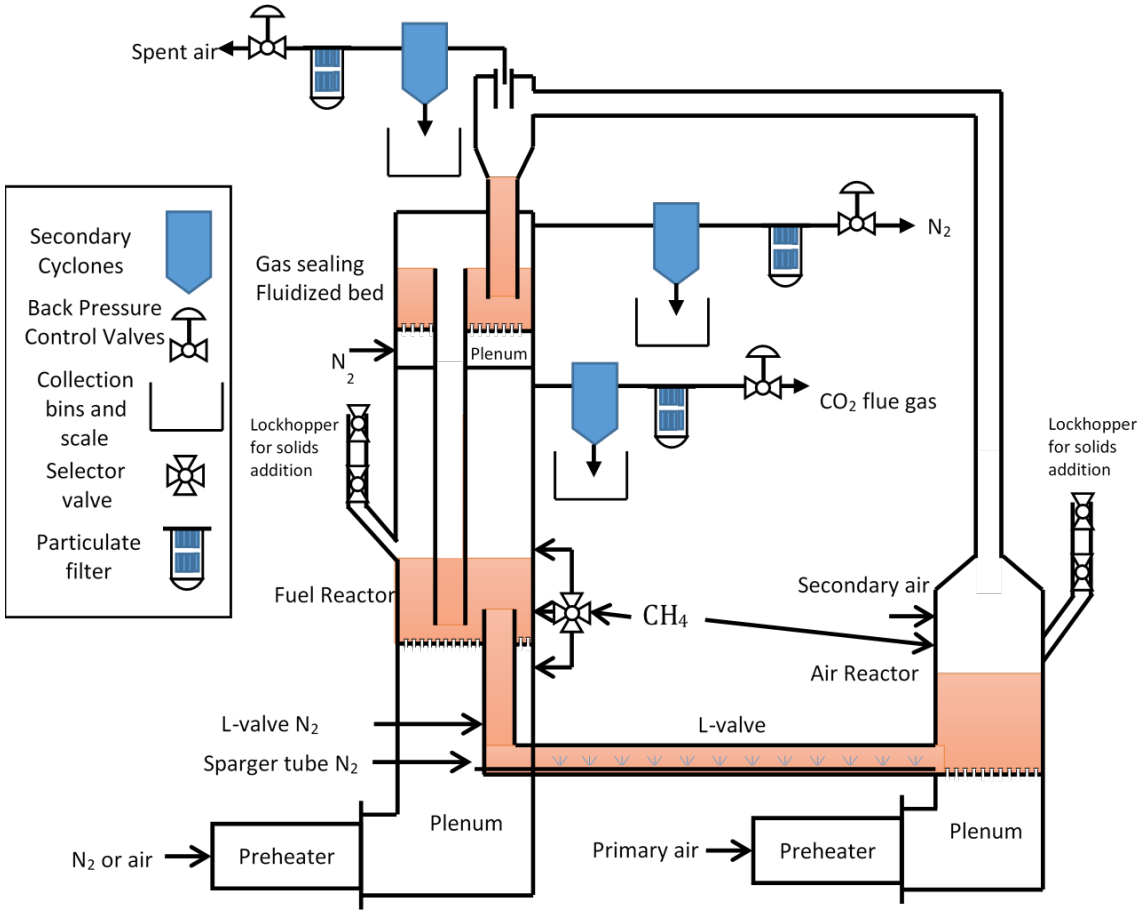

FIGURE 2. SETUP OF NETL'S 50 KW_{TH} CHEMICAL LOOPING REACTOR.

The fuel reactor in NETL's Chemical Looping Reactor uses a mixture of natural gas and nitrogen diluent[1] to fluidize the oxygen carrier material. The oxygen carrier from the fuel reactor drains into an L-valve which conveys solids to the air reactor. The circulation rate that can be achieved through an L-valve is a function of the pressure profile through the L-valve. By using an underflow standpipe in the fuel reactor, the pressure at the L-valve inlet will vary with the bed height in the fuel reactor. The back-pressure control valve on the fuel reactor gas outlet also provides some pressure and subsequent carrier circulation rate control. When the oxygen carrier material from the L-valve reaches the air reactor, it is fluidized using the primary air flowing through a bubble cap distributor. Secondary air is also injected into the air reactor to elutriate the oxidized carrier material into the riser. This secondary air flow helps transport oxygen carrier particles through the riser section and reduces slugging flow transport events. After the oxygen carrier material is vertically transported through the riser, the solids are horizontally transported through the crossover and into the cyclone where the solids are separated from the vitiated air. The oxygen carrier flows through a cyclone dip-leg and into the seal pot. Finally, the loop is completed when the solids overflow from the loop-seal and re-enter the fuel reactor.

All of the gas flows into the NETL CLR test facility are independently controlled using mass flow controllers (Alicat Scientific). Most of the inlet gas flows are also electrically preheated and controlled using PID temperature controllers. The fluidizing gases for the air reactor and the fuel reactor can be preheated to achieve reactor gas temperatures in the 600-700°C range. Similarly, the secondary air can be preheated to approximately 600°C.

The startup procedure for the NETL CLR test facility includes a gradual preheating schedule as recommended by the refractory manufacturer (i.e., ~50°C/hr). The electric preheaters can match this heating rate very closely until the reactor temperatures reach 600-700°C. Air is used during the preheating phase for both the fuel and air reactors. Initially, there is no oxygen carrier material in the unit, so there are no solids handling issues during the preheating phase. After the fuel and air reactors have reached the 600-700°C range, natural gas will auto-ignite when introduced into the air reactor and fuel reactor.

The test facility has the capability to inject natural gas into both the air reactor and the fuel reactor for natural gas augmented preheating. For flexibility in operation, the natural gas injection location can also be changed using external selector valves. The fuel injection locations in the fuel reactor include: 1) Into the dense fluidized bed region, 2) Upstream of the distributor plate, or 3) Above the fluidized bed region. The fuel injection locations in the air reactor include 1) Into the dense fluidized bed region, and 2) Above the dense bed region.

In order to transition from natural gas augmented preheating to chemical looping combustion, the following steps are taken in the fuel reactor: 1) The fuel flow is temporarily stopped, 2) the fluidizing gas (air during preheat) is ramped to zero flow, and at the same time, a new fluidizing gas (nitrogen during CLC testing) is ramped to a predetermined flow setpoint, 3) The fuel injection location is set to inject fuel upstream of the distributor plate, and 4) The fuel flow is re-established at a predetermined flow setpoint. The fuel injection upstream of the distributor plate allows some mixing time with the fluidization gas prior to entering the fluidized bed through the bubble caps. In the air reactor, the fuel flow can be stopped during chemical looping combustion periods to achieve a so-called "auto-thermal" operation, or the fuel flow in the air reactor can be used to maintain a constant air reactor temperature during chemical looping combustion periods. Achievement of an auto-thermal state is important, since the energy input for a real chemical looping system needs to come from the oxidation and reduction of the oxygen carrier and not from external heaters. Both of

[1] *In a commercialized unit, the nitrogen diluent would be replaced with steam and/or carbon dioxide. Nitrogen is used in this unit only since it is more readily available than steam in terms of utilities.*

these operating modes have been achieved in the NETL CLR test facility, and the data from this specific test will be described in more detail in subsequent sections of this report.

The gas sampling and analysis system is an important part of this test facility. The gas sample conditioning equipment includes particulate removal, moisture removal, and pressure controls for the gas analyzer manifold. An in-line sintered metal filter is used to remove dust and particulates. Commercial sample conditioners (Baldwin Environmental and Universal Analyzer) are used to cool the sample stream to 4°C, and continuously remove condensate using peristaltic pumps. From the gas sample conditioners, the clean, dry sample stream flows through continuous emission gas analyzers. Some gas analyzers can be sensitive to changes in the inlet pressure and flow, so small pressure controllers (Alicat Scientific) are used to maintain a constant inlet pressure to the gas analyzers. The outlet pressure of the gas analyzers is very close to atmospheric pressure.

Since the exhaust gas composition is used to assess performance parameters like fuel conversion, mass closure, and oxygen utilization, the gas analysis system plays an important role in the data analysis. The gas composition for each of the reactor outlet streams are analyzed. Gas samples are extracted from the air reactor, fuel reactor, and seal pot vent lines continuously. For each of these sample locations, the measured gas components are listed in Table 1. Most of the continuous emission gas analyzers utilize a non-dispersive infrared (NDIR) sensing approach. For the oxygen composition, paramagnetic sensors have been used to prevent potential interference that can occur using an electrochemical sensor when gas species such as CO, H_2, and CH_4 are present in the gas sample stream. The on-line gas chromatograph (GC) provides a quality check on many of the measured gas components, and in addition the micro-GC also measures nitrogen and hydrogen present in the fuel reactor exhaust. All of these gas analyzers, including the micro-GC, are calibrated prior to the test using a suite of calibration gases.

TABLE 1: GAS ANALYZER SPECIFICATIONS

	Gas Species / Sensor	Analyzer	Range	Interval Between Samples
Air Reactor	CO_2 - NDIR O_2 - Paramagnetic	Siemens Ultramat 23	0-25% 0-100%	1 sec
Seal pot	CO_2 – NDIR	Horiba VIA-510	0-1%	1 sec
Fuel Reactor	CH_4 - NDIR CO_2 - NDIR	Siemens Ultramat 23	0-25% 0-50%	1 sec
	CO - NDIR	Horiba VIA-510	0-4%	1 sec
	O_2 - Paramagnetic	M&C PMA 12	0-100%	1 sec
	CO, CO_2, CH_4, O_2, N_2, H_2 – Thermal Conductivity Detector	Inficon 3000 MicroGC	0-100%	90 sec

2.2 Properties of the Cu/Fe Oxygen Carrier

NETL researchers have been developing oxygen carrier materials for chemical looping combustion applications[6,7,8]. The Cu/Fe/alumina oxygen carrier material used in this test campaign is actually the second generation version of this material composition. The first generation material was manufactured using a spray-drying technique which utilized expensive precursors. In an attempt to find more economical approaches and to achieve a slightly larger particle size distributions, the second generation material was developed. The second-generation oxygen carrier is produced using a mixing-tumbling technique. A rotary drum is used to mix moisture and dry powder precursors. After the particles agglomerate into particles of the desired particle size, they are sintered at high temperature to achieve the desired mechanical properties. This wet agglomeration technique produces an oxygen carrier material with a larger particle size and theoretically a lower manufacturing cost than the first generation carrier material.

As shown in Table 2, the formulation consists of roughly 30% iron oxide (Fe_2O_3), 40% copper oxide (CuO) and the balance being alumina (Al_2O_3) by weight. The presence of copper oxide gives the material some oxygen uncoupling properties, which is beneficial to conversion of the fuel. Copper, and a few other materials, will directly release oxygen into the gas phase when the oxygen partial pressure is very low. When the oxygen is no longer coupled to the lattice structure, the oxygen reacts much faster. The term oxygen uncoupling is used to describe the direct release of oxygen from the solid lattice. The oxygen carrier material used in this test has some oxygen uncoupling characteristics, but other oxygen transport mechanisms are also possible using this oxygen carrier material.

The hydrodynamic characteristics of the second generation oxygen carrier material are also summarized in Table 2. The hydrodynamic characteristics of the carrier are estimated both using laboratory techniques (minimum fluidization velocity, U_{mf}) and well-known correlations (terminal velocity, U_t). The minimum fluidization velocity has been measured by filling the seal pot with a known weight of oxygen carrier material and gradually ramping the fluidizing gas until the bed pressure drop stops increasing with flow (see Figure 3). The minimum flow rate at which the pressure curve becomes independent of the fluidization gas flow is the point of minimum fluidization. The minimum fluidization velocity measured in the actual seal pot is slightly lower than the velocity measured in a more controlled laboratory setup. However, both of these velocities are reasonably close to 0.1 m/s. Other particle characteristics are also listed in Table 2.

TABLE 2. HYDRODYNAMIC AND CHEMICAL PROPERTIES OF THE SECOND-GENERATION COPPER-IRON OXYGEN CARRIER.

Property	Value	Units	Source
Hydrodynamic Characteristics			
Particle Size Range	213-582	μm	Measured (Sympatec QICPIC)
Sauter Mean Diameter (d_{32})	343	µm	Measured (Sympatec QICPIC)
Sphericity	0.91	--	Measured (Sympatec QICPIC)
Particle density	2900	kg/m^3	
Particle skeletal density	4730	kg/m^3	Helium pycnometry
Bulk density	1430	kg/m^3	Measured from seal pot fluid bed experiment
Minimum Fluidization Velocity	0.14	m/s	Measured at 26°C in a small fluidized bed

	0.09	m/s	Measured from seal pot fluid bed experiment
Terminal Velocity (25°C)	2.36	m/s	Textbook correlation[9]
Terminal Velocity (900°C)	2.52	m/s	Textbook correlation[9]
Chemical Characteristics			
Fe_2O_3	31.32	wt%	XRF analysis
CuO	37.49	wt%	""
Al_2O_3	31.19	wt%	""

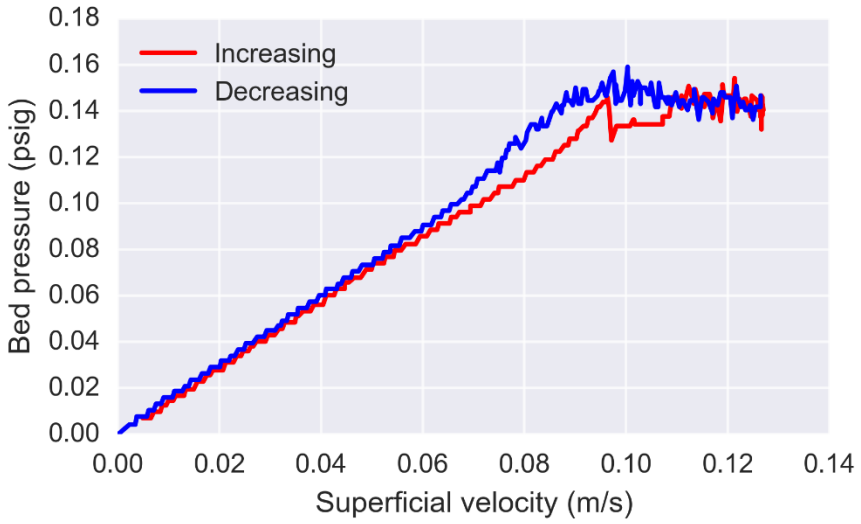

FIGURE 3. SAMPLE CURVE OF THE ROOM-TEMPERATURE LOOP-SEAL TESTS USED FOR MEASURING THE MINIMUM FLUIDIZATION VELOCITY.

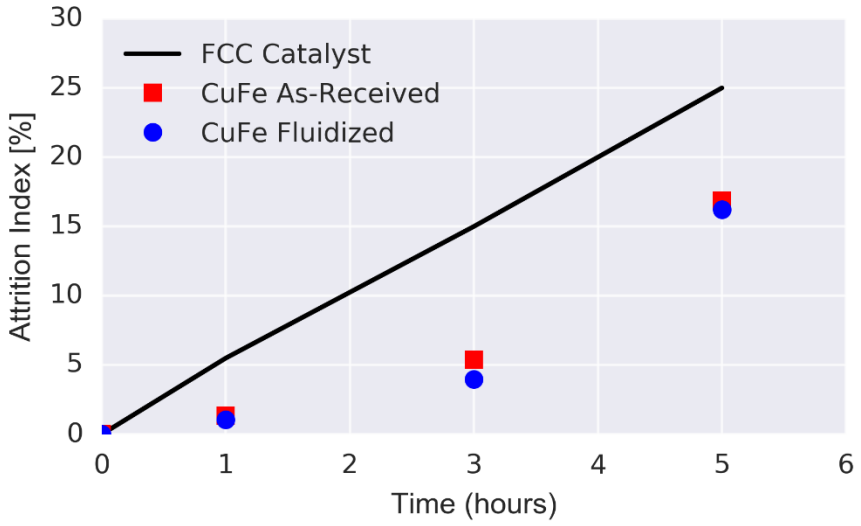

FIGURE 4: ATTRITION DATA OF AS-RECEIVED MATERIALS

A standard test method (ASTM D5757[10]) is utilized to determine the attrition and abrasion resistance of the as-received oxygen carrier materials (see Figure 4). Since this test method is commonly used for fluid catalytic cracking (FCC) catalysts, data from a baseline FCC catalyst is shown as a reference. A lower

attrition index is desired for a more durable oxygen carrier material. These tests are conducted at room temperature using air from a site compressed air supply. NETL's second generation Cu/Fe carrier material demonstrates a slightly better attrition index than the first generation material and both are better than the standard FCC catalyst. However, during some room temperature fluidization testing in the seal pot, fines were observed coming from the bed at relatively low fluidization velocities ($U_g < 1.2\ U_{mf}$). After an hour of fluidization, fines were still observed coming from the fluidized bed.

Figure 5 shows the particle size distribution of the second generation Cu/Fe carrier material before and after fluidization in the seal pot at room temperature. The light fluidization caused the particle size distribution of the carrier material to shift to the left which is indicative of a decrease in particle size. In addition, a small but noticeable peak appears in a size range below 100 microns. This is a characteristic of particle surface abrasion[11]. Although this particle abrasion did not significantly affect the overall integrity of the particle, fines were continuously observed during the hot testing. These fines produced large pressure drops across the filters on each of the gas outlets, and frequent filter changes were required.

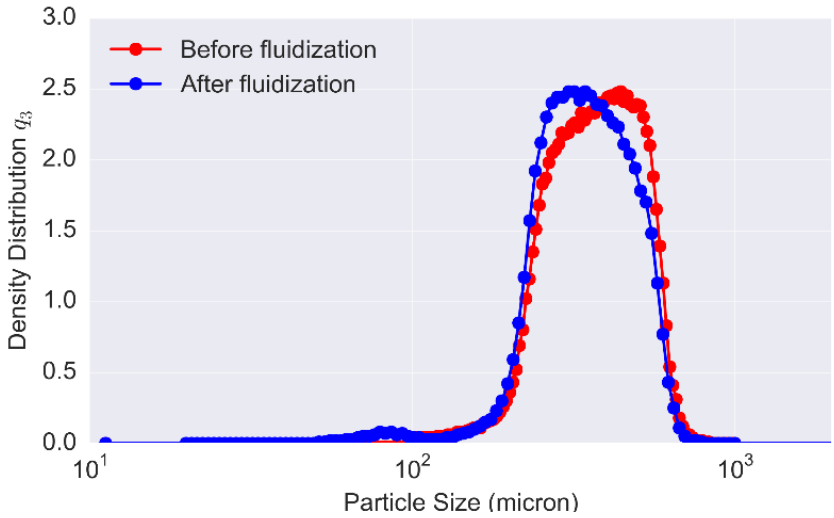

FIGURE 5. PARTICLE SIZE DISTRIBUTION BEFORE AND AFTER ROOM-TEMPERATURE FLUIDIZATION TESTS.

2.3 Data Analysis Procedure

In this section, the performance metrics are defined in terms of process data collected during the test campaign. This section also discusses the assumptions that have been made in the analyses. Other information to support the assumptions are discussed as appropriate. The following sections will define performance metrics such as fuel conversion, mass closure, mean residence times, and oxygen carrier conversion.

2.3.1 Molar Flowrates of Wet Flue Gas Species

The molar flowrate of CH_4, CO_2, and CO exiting the fuel reactor are estimated using measured gas concentrations in the fuel reactor outlet stream. This analysis assumes that all of the nitrogen flowing into the fuel reactor as a fluidizing gas leaves the fuel reactor and behaves as an inert gas. In other words, inter-reactor leakage is neglected, and there is evidence to suggest that this assumption is a reasonable approximation for this test campaign.

The estimate involves calculating the dry outlet flowrate of gases exiting the fuel reactor by dividing the measured flowrate of nitrogen entering the fuel reactor by the nitrogen mole (volume) fraction of the gas exiting the fuel reactor, or:

$$Q^*_{\mathrm{T,dry}} = \frac{Q^*_{\mathrm{N_2,in}}}{y_{\mathrm{N_2,out,dry}}} \quad (1)$$

Where $Q^*_{\mathrm{T,dry}}$ and $Q^*_{\mathrm{N_2,in}}$ are the total outlet and nitrogen inlet standard (*) volumetric flow rates, and $y_{\mathrm{N_2,out,dry}}$ is the dry mole fraction of nitrogen in the fuel reactor exhaust.

Once the dry outlet volumetric flowrate is known, the molar flowrate of the individual gas species is calculated:

$$\dot{N}_{i,\mathrm{out}} = Q^*_{\mathrm{T,dry}} y_{i,\mathrm{out,dry}} \frac{\rho_{i,\mathrm{STD}}}{MW_i} \quad (2)$$

Where $i = CO_2$, CO, CH_4, H_2, and N_2, $\rho_{i,\mathrm{STD}}$ is the density of species *i* at standard temperature and pressure (25°C, 101.3 kPa), and MW_i is the molecular weight of species *i*.

During this test campaign, the natural gas composition was analyzed on three different days, and the CH_4 concentration in the natural gas was 96.7 $\pm$ 0.2%. In this report, the natural gas fuel is treated as methane, and the natural gas analyses suggest that this is a reasonable approximation.

If all of the hydrogen entering the fuel reactor exits the fuel reactor in the form of steam, methane, and hydrogen, then the steam molar flow rate can be calculated by subtracting the moles of CH_4 and H_2 in the outlet from the moles of CH_4 entering the reactor:

$$\dot{N}_{\mathrm{H_2O,out}} = 2\dot{N}_{\mathrm{CH_4,in}} - 2\dot{N}_{\mathrm{CH_4,out}} - \dot{N}_{\mathrm{H_2,out}} \quad (3)$$

Once the molar flow rate of water vapor in the outlet is calculated, then the total molar flowrate of the flue gas can be calculated as the sum of the molar flowrates of the dry products and the molar flow rate of water vapor, $\dot{N}_{\mathrm{T,out}}$. The wet gas mole fractions can be also be calculated (see Equation 4).

$$y_{i,\mathrm{out}} = \frac{\dot{N}_{i,\mathrm{out}}}{\dot{N}_{\mathrm{T,out}}} \quad (4)$$

Thus, the standard wet volumetric flowrate of flue gas exiting the fuel reactor is

$$Q^*_{\mathrm{T,wet}} = \frac{Q^*_{\mathrm{T,dry}}}{1 - y_{\mathrm{H_2O,out}}} \quad (5)$$

2.3.2 Carbon Balance

One approach to assess the amount of inter-reactor leakage that may be occurring between the fuel reactor and the air reactor is a carbon balance that can compare the total moles of carbon leaving the fuel reactor to the total moles of carbon entering the fuel reactor. This calculation would also identify extensive carbon deposition, if the carbon balance was poor. The carbon balance term is calculated by dividing the total molar flowrate of carbonaceous gases out by the molar flowrate of CH_4 in:

$$C_{\mathrm{bal}} = \frac{\dot{N}_{\mathrm{CH_4,out}} + \dot{N}_{\mathrm{CO_2,out}} + \dot{N}_{\mathrm{CO,out}}}{\dot{N}_{\mathrm{CH_4,in}}} \quad (6)$$

This parameter needs to be as close to one as possible to ensure good carbon balance closure, and for most of this test campaign this value was in the range of 0.95 – 1.07. This analysis assumes that the natural gas can be approximated as CH_4, and as discussed above, the CH_4 concentration in the natural gas fuel has been measured at 96.7 $\pm$ 0.2%. Other factors that can affect this calculation include the pressure and flows

through the continuous emission gas analyzers. Although considerable effort is made to control these factors, particulate buildup on the in-line filter can affect the quality of the gas composition measurements.

2.3.3 Methane Conversion

In this test, the conversion is calculated in two ways. The first approach is based on the disappearance of methane, whereby the conversion is the moles of methane consumed divided by the moles of methane entering the fuel reactor (see Equation 7).

$$X_{\mathrm{CH_4}} = \frac{\dot{N}_{\mathrm{CH_4,in}} - \dot{N}_{\mathrm{CH_4,out}}}{\dot{N}_{\mathrm{CH_4,in}}} \tag{7}$$

The second method is based on the molar flowrate of CO_2 in the flue gas, which is more indicative of the selectivity of the conversion of gas to CO_2. Since CO_2 is the desired product for complete combustion, this methane conversion is calculated by dividing the molar flowrate of CO_2 in the flue gas by the molar flowrate of methane fed to the fuel reactor:

$$X_{\mathrm{CH_4 \rightarrow CO_2}} = \frac{\dot{N}_{\mathrm{CO_2,out}}}{\dot{N}_{\mathrm{CH_4,in}}} \tag{8}$$

If a significant fraction of fuel is converted to CO or carbon, instead of CO_2, then the first approach would bias the calculated conversion toward higher values than the second approach.

2.3.4 Solids Circulation Rate

The solids circulation rate is an important parameter for understanding the performance details of a specific oxygen carrier material and chemical looping combustion systems in general. This quantity is also very difficult to measure. Several approaches have been proposed to infer the solids mass flowrate from pressure drop measurements (i.e., riser, cross-over, cyclone, etc.), but calibrating these techniques at operating conditions is not trivial. In this test campaign, an approach to correlate the pressure drop across the top cross-over involves a transient analysis of the system response to a perturbation. This method is used to develop a correlation between pressure drops in the fluidized beds and other pressure drops that could be used to infer a solids circulation rate in the system. This approach will be described in more detail in the following paragraphs.

The basis for this approach is the relationship between the pressure drop across a fluidized bed and the mass of the bed (see Equation 9). This relation assumes that the bed is fully fluidized, so the pressure drop is independent of the flow through the bed. Since the fluidizing gas velocities are several times larger than the minimum fluidization velocity, this assumption is valid.

$$m_{\mathrm{bed},i} = \frac{\Delta P_i A_i}{g} \tag{9}$$

Where ΔP_i is the bed pressure drop across reactor *i*, A_i is the cross-sectional area of the reactor *i*, and g is the acceleration of gravity. Taking a time derivative of Equation 9, the mass flow rate of solids that accumulate in the reactor is directly related to the rate of change in bed pressure drop (see Equation 10).

This analysis assumes that the oxygen carrier circulation between the fuel reactor and the air reactor can be stopped.

$$\frac{dm_{\mathrm{bed},i}}{dt} = \frac{A_i}{g} \cdot \frac{d\Delta P_i}{dt} \qquad (10)$$

In order to stop the oxygen carrier circulation, the aeration flows in the L-valve are decreased. Since the air reactor continues to transport solids through the riser, the pressure drop across the air reactor bed will decrease at a rate that is proportional to the mass flow rate of solids leaving the air reactor (see Figure 6). Conversely, the pressure drop across the fuel reactor will increase at a rate that is proportional to the mass flow rate of solids accumulating in the fuel reactor. Due to its smaller cross-sectional area, the air reactor pressure drop is a more sensitive indication of the solids circulation rate, so the air reactor pressure drop is used in subsequent calculations.

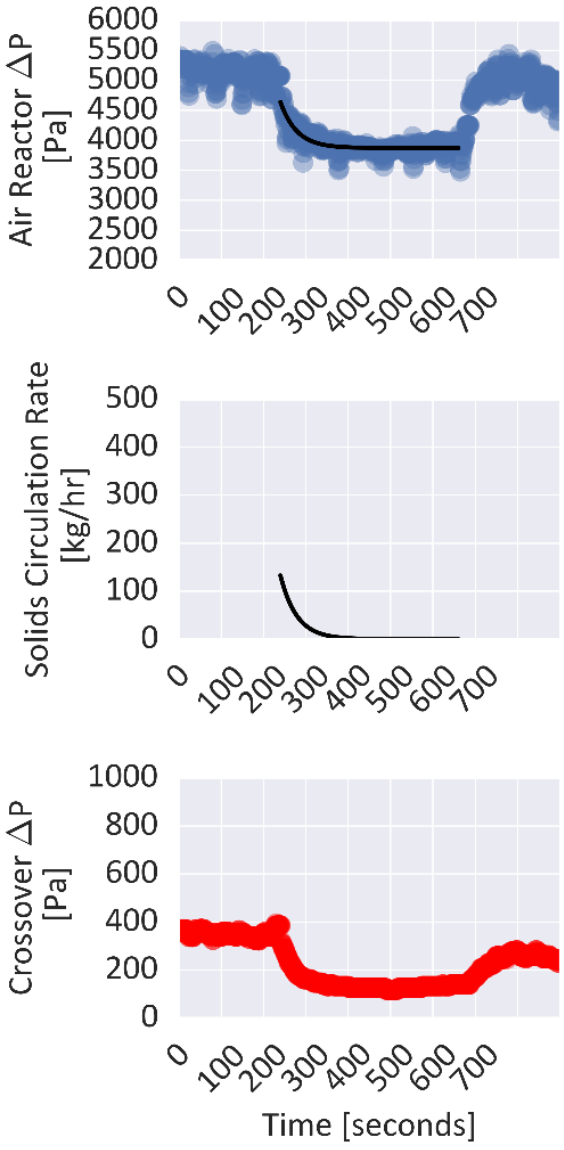

FIGURE 6: TRANSIENT RESPONSE OF THE AIR REACTOR BED PRESSURE DROP (TOP) AND CROSS-OVER PRESSURE DROP (BOTTOM). THE MIDDLE FIGURE IS A PLOT OF THE SOLIDS CIRCULATION RATE CALCULATED BASED ON THE LEAST-SQUARES FIT TO THE AIR REACTOR BED PRESSURE DROP.

After the aeration flows to the L-valve are stopped, the oxygen carrier material in the air reactor is transported to the fuel reactor until a new steady-state bed height is achieved. By calculating the derivative of the bed pressure drop during this transition, the oxygen carrier circulation rate as a function of time can be calculated. However, the bed pressure drop for a fluidized bed typically contains a lot of noise, so some method is required to deal with the noise in the signal before the time derivative is calculated. Therefore, an exponential function is fit to the bed pressure drop using a least-squares optimization algorithm. The expression derived from the least-squares fit is differentiated at each time and the corresponding carrier circulation rate is calculated using Equation 10.

The final step is to correlate another indicator for the solids circulation rate (e.g. the crossover pressure drop). After examining all of the transient tests performed during this test campaign only two conditions met all of the conditions and requirements that will be described in more detail in the discussion of results. The measured correlation between the cross-over pressure drop and solids circulation rate during this transient testing is shown in Figure 7.

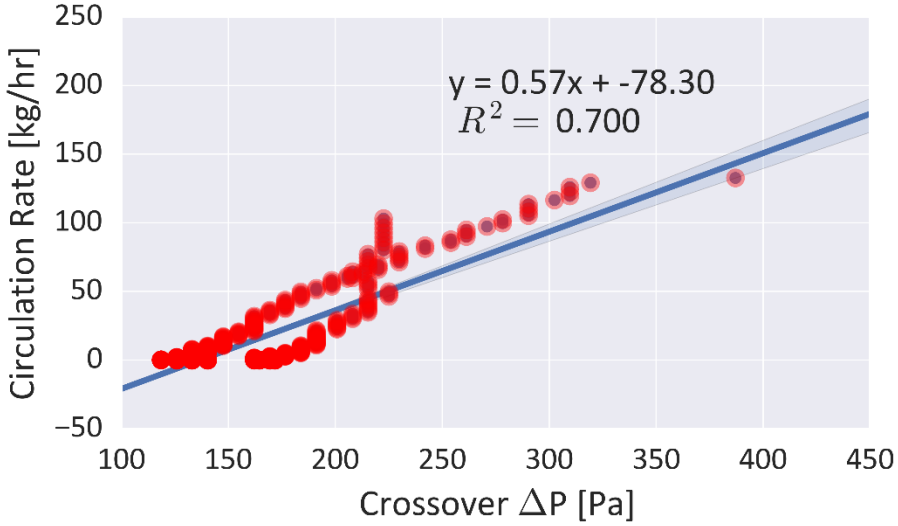

FIGURE 7. CORRELATION BETWEEN CROSS-OVER PRESSURE DROP AND SOLIDS CIRCULATION RATE

For the remainder of this report, the solids circulation rate $\dot{m}_{\mathrm{OC}}$ is determined from a correlation of the pressure drop across the riser crossover section ΔP_{CR}, assumed linear, where a and b are constants derived from a regression analysis of these transient tests.

$$\dot{m}_{\mathrm{OC}} = a \cdot \Delta P_{\mathrm{CR}} + b \tag{11}$$

2.3.5 Oxygen Carrier Conversion

This parameter depends on the oxygen carrier material, the oxygen carrier circulation rate, and several other assumptions. First, assuming that inter-reactor leakage is negligible, the molar flow rate of oxygen consumed by the methane in the fuel reactor, or oxygen leaving the reactor, can be calculated. The molar flow rate of oxygen (atomic oxygen basis) is calculated using the measured and/or calculated molar flow rates of CO_2, CO, and H_2O (see Equation 12). Note that an atomic oxygen basis is used in Equation 12 to be consistent with the solids oxygen transport assumptions in subsequent equations.

$$\dot{N}_{\mathrm{O,out}} = \dot{N}_{\mathrm{H_2O,out}} + 2\dot{N}_{\mathrm{CO_2,out}} + \dot{N}_{\mathrm{CO,out}} \tag{12}$$

The oxygen transport capacity of the oxygen carrier depends on the chemical composition of the oxygen carrier and the solids circulation rate ($\dot{m}_{\mathrm{OC}}$) for the oxygen carrier material. As described in the previous section, there is error in the solids circulation rate for the oxygen carrier material.

In order to calculate the maximum oxygen transport capacity for the carrier material, some assumptions have been made. With the exception of the alumina (Al_2O_3) that is considered to be inert phase, Equation 13 assumes that all the oxygen contained in the Cu/Fe material can be released. This analysis also assumes that the oxygen carrier material is fully re-oxidized in the air reactor. The weight fractions of active metal (i.e., Cu and Fe) oxides are denoted as f_i, (where $i = \mathrm{Fe_2O_3}$, CuO), and the values listed in Table 2 are used in the analysis. The respective molecular weights of the oxidized active metal oxides are denoted as MW_i.

$$\dot{N}_{\mathrm{O,total}} = \dot{m}_{\mathrm{OC}} \left(\frac{3 f_{\mathrm{Fe_2O_3}}}{MW_{\mathrm{Fe_2O_3}}} + \frac{f_{\mathrm{CuO}}}{MW_{\mathrm{CuO}}} \right) \tag{13}$$

Thus, the oxygen carrier conversion is then

$$X_{OC} = \frac{\dot{N}_{\mathrm{O,out}}}{\dot{N}_{\mathrm{O,total}}} \tag{14}$$

2.3.6 Average Fuel Reactor Gas Residence Time

The gas residence time in the fuel reactor is an important independent parameter for chemical looping combustion due to its impact on the fuel conversion. Since the oxygen carrier material transports oxygen into gas phase products (i.e., CO_2, CO, H_2O), the flow of gaseous products leaving the fuel reactor is higher than the mass flow rate of gaseous reactants entering the reactor. These heterogeneous chemical reactions can cause a significant increase in volumetric flow rate, and gas velocity. Therefore, the gas residence time is calculated based on an average of the inlet flow rate and the outlet flow rate. The log-mean average is chosen because the product gases (assuming a packed bed behavior) cause the gas velocity to increase as a function of height in the reactor. The log-mean flow rate is:

$$Q_{\mathrm{LM}} = \frac{Q_{\mathrm{T,wet}} - Q_{\mathrm{in}}}{\ln\left(\frac{Q_{\mathrm{T,wet}}}{Q_{\mathrm{in}}}\right)} \tag{15}$$

Where

$$Q_{\mathrm{T,wet}} = \frac{\dot{N}_{\mathrm{T,out}} R T_{\mathrm{FR}}}{P_{\mathrm{FR}}} \tag{16}$$

Where *R* is the ideal gas constant, T_{FR} is the actual fuel reactor temperature, and P_{FR} is the fuel reactor pressure. If the average gas velocity in the fuel reactor is:

$$U_{\mathrm{g,LM}} = \frac{Q_{\mathrm{LM}}}{A_{\mathrm{FR}}} \tag{17}$$

Then the average gas residence time in the fuel reactor bed is:

$$\tau_{\mathrm{g,FR}} = \frac{h_{\mathrm{bed,FR}}}{U_{\mathrm{g,LM}}} \tag{18}$$

where $h_{\mathrm{bed,FR}}$ is the bed height, estimated from the pressure drop as described below. This residence time calculation assumes that fuel reactor fluidized bed behaves like a packed bed.

2.3.7 Bed Height

The bed heights are calculated based on fluidization tests that are conducted prior to the hot test campaign. If the bed material is fluidized, then the relationship between the bed pressure drop and the bed height should be linear. As mentioned previously, ambient temperature fluidization tests are used to develop a correlation between the bed pressure drop and the bed height. The correlation for the second generation Cu/Fe oxygen carrier material is listed in Equation 19.

$$h_{\mathrm{bed},i}[\mathrm{in}] = 1 + 26.667 \Delta P_i[\mathrm{psid}] \tag{19}$$

The intercept value comes from the fact that the bottom pressure tap is one inch above the distributor plate.

2.3.8 Solids Residence Time

The solids residence time is calculated from knowledge of the mass of oxygen carrier material in the bed and the oxygen carrier flow rate $\dot{m}_{\mathrm{OC}}$. The solids inventory was estimated from the bed height in Equation 19, multiplied by the cross sectional area and bulk density at fluidization.

$$m_{\mathrm{bed,FR}} = \rho_{\mathrm{B}} A_{\mathrm{FR}} h_{\mathrm{bed,FR}} \tag{20}$$

The solids residence time is simply the ratio of the bed mass and the oxygen carrier circulation rate. The data analysis to estimate the solids circulation rate has been described in a previous section.

$$\tau_{\mathrm{OC,FR}} = \frac{m_{\mathrm{bed,FR}}}{\dot{m}_{\mathrm{OC}}} \tag{21}$$

This expression assumes plug-flow reactor behavior, which is a valid assumption based on the slugging nature of the tall, narrow diameter fluidized beds in the system.

3. OBSERVATIONS

3.1 Operational Summary

An overall summary of the reactor temperatures, pressures, and estimated solids is shown in Figure 8. This test campaign started on July 10, 2016 and continued for 5 days and 10 hours. As previously described, the electrical preheating is used to gradually heat the refractory in accordance with manufacturers' specifications. When the reactor temperatures exceed the auto-ignition temperature, natural gas is introduced into both the fuel and air reactors. At approximately 11:45 a.m. on July 11, an over-temperature condition in the air reactor stopped the fuel flow. Following a purge cycle, the natural gas flows were re-established and preparations were made for adding oxygen carrier material to the system.

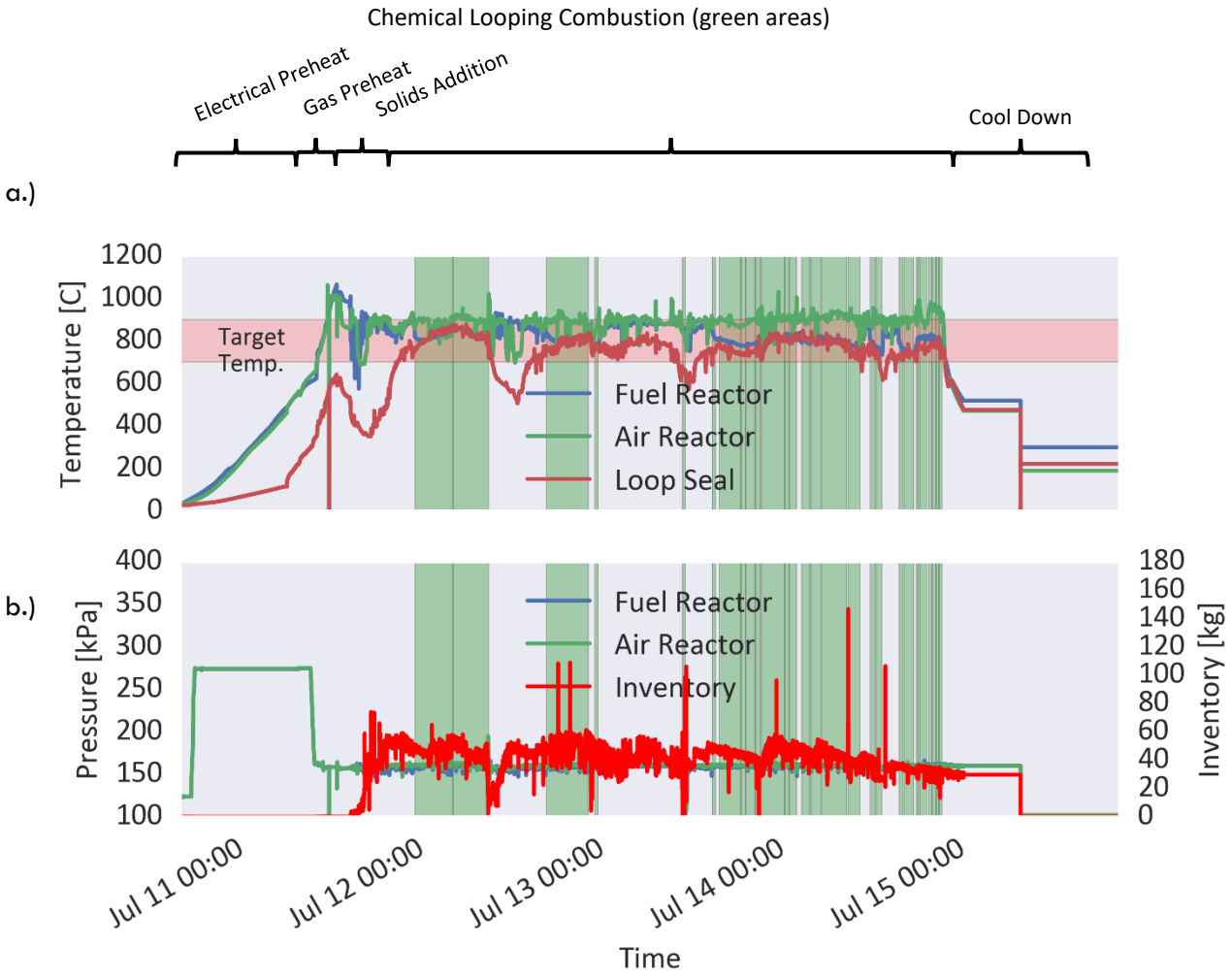

FIGURE 8. OPERATIONAL SUMMARY. (A) REACTOR TEMPERATURES, (B) SOLIDS INVENTORY AND REACTOR PRESSURES. GREEN BOXES CONSIST OF CHEMICAL LOOPING TRIALS.

At approximately 13:30 on July 11, the first batches of oxygen carrier material were added to the fuel reactor using a lock-hopper system (see Figure 2). The initial batches were small (0.9 kg) to reduce the thermal shock to the refractory. At approximately 15:00 on July 11, larger (2.3 kg) batches were added and the oxygen carrier inventory increased as shown by the red line in Figure 8(b). The target solids inventory was 55 kg.

Solids circulation began slowly and 4 days 8 hours of hot solids circulation were accumulated during this test. Once the solids circulation and the reactor temperature targets were achieved, the air in the fuel reactor was replaced with nitrogen, and chemical looping combustion periods were performed. The Chemical Looping Combustion periods are indicated by the green areas in Figure 8. For this test campaign, a cumulative total of 40 hours of chemical looping combustion were completed.

There were two upset conditions encountered during this test. The first upset condition occurred the morning of July 12 when a pressure upset caused the loss of 27 kg of the carrier in a period of less than 5 minutes. This upset occurred while the back pressure control valves were being tuned. During the morning of July 13, the entire unit was intentionally shutdown to install a purge on a pressure transmitter impulse line. Particulate buildup in this impulse line was causing pressure control issues. For example, the level of noise in the oxygen carrier inventory (see Figure 8b, red line) increased until the nitrogen purge was installed to clean this port.

The gradual loss of carrier from the system can also be observed from the oxygen carrier inventory trend in Figure 8b. Fines were captured in the secondary cyclones and downstream filters, and frequent filter changes were required. On the average, approximately 1.4 kg/hr of solids were lost from the system. This will be discussed in more detail later in this section.

3.2 Transient Tests For Determining Circulation Rates

As previously described, a series of transient tests were performed to generate calibration curves of oxygen carrier circulation rate as a function of other system parameters (i.e., crossover pressure drop). The bed pressure drop in the air reactor decayed exponentially, so Equation 22 was used to model the transient air reactor bed pressure drop response. The decay constant, k, between the initial and final states was calculated using a least-squares optimization algorithm. The least-squares regression was differentiated to find the oxygen carrier circulation rate as described in Section 2. The goal of these transient tests was to correlate the solids circulation rate to another process variable that was used to infer the solids circulation rate for steady-state conditions. For the purposes of this report, the crossover pressure drop was selected as the key process indicator for the solids circulation rate.

$$\Delta P_i(t) = \Delta P_1 + (\Delta P_0 - \Delta P_1)e^{-k(t-t_0)} \quad (22)$$

ΔP_0 and t_0 are the initial pressure drop and time, respectively. ΔP_1 is the final bed pressure drop, and, k is the fit parameter. The transient tests that were used to develop the correlation between oxygen carrier circulation rate and crossover pressure drop are shown in Figure 9. These two transient test periods represent "acceptable" data sets and the bed pressure drops and the aeration flows are shown. Figure 9 shows that the aeration gas flow was reduced quickly, but no significant bed pressure disturbances were generated as a result of reducing the aeration gas flows to the L-valve.

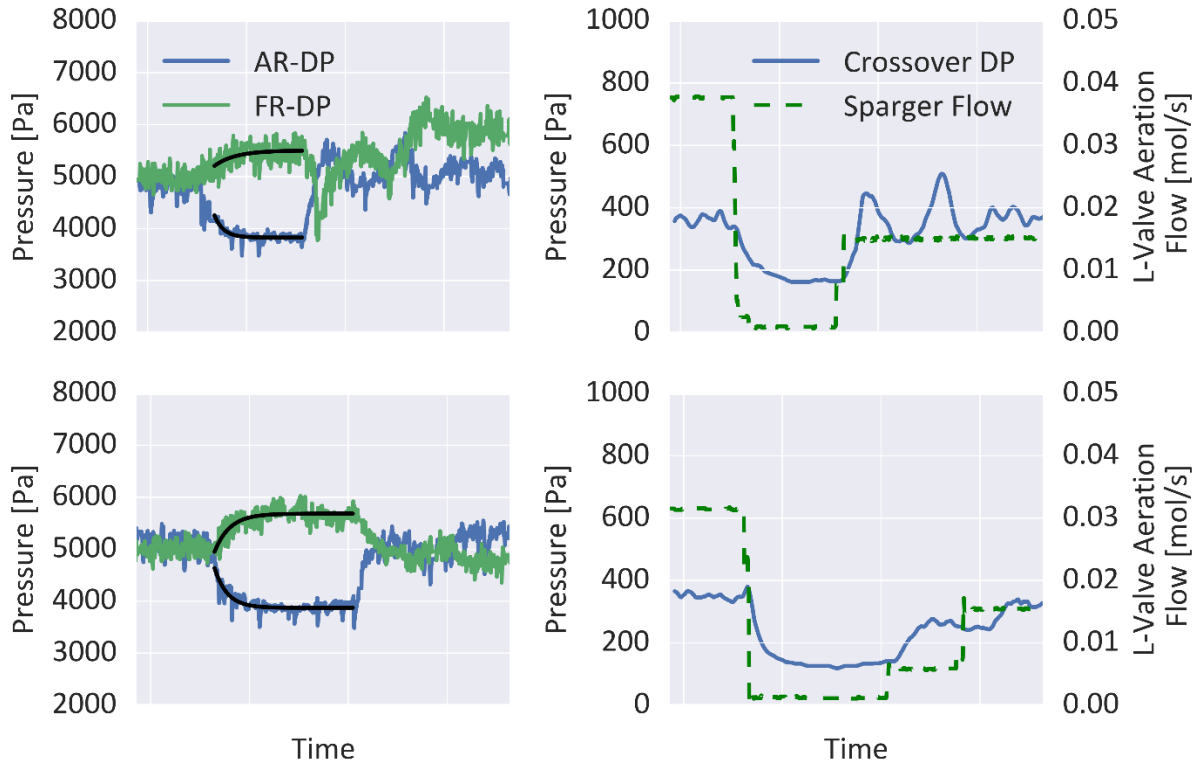

FIGURE 9: TRANSIENT L-VALVE AERATION GAS CUTOFF TESTS USED FOR DETERMINING AN ESTIMATION OF SOLIDS CIRCULATION RATE.

Although the technique and data analysis approach was described in Section 2, this section discusses some of the lessons learned during this test campaign. Some qualitative requirements have been identified to improve the quality of these datasets. In the future, these transient response tests need to meet the following requirements:

1) The perturbation needs to stop the oxygen carrier circulation. If the solids flow between the fuel reactor and the air reactor does not stop, then the calculated solids circulation rate would be under-estimated. In general, the crossover pressure drop should also decay to sufficiently small values to indicate no solids circulation.
2) The perturbation should not be too fast or too large that a pressure upset condition is introduced. If the perturbation causes a pressure surge, or upset, the bed pressure drops change significantly from the initial steady-state level.
3) The perturbation should not be too slow. If the perturbation is too slow, then bed pressure drop at the time when the solid circulation stops may be significantly different from the initial state.
4) Both the bed pressure drop and the crossover pressure drop need to be at an initial steady-state condition. If this transient test is performed when the system is not at a stable, steady-state condition, then significant uncertainties can be introduced in the regression equation.

A transient test that did not meet the last requirement listed above is shown in Figure 10. Although the regression fit to the data was reasonable, there were several qualitative features that question the validity of this dataset. For example, the initial condition was not at a stable, steady-state condition. When the perturbation was initiated at 240 seconds, the crossover pressure drop was decaying. As a result, the initial rate of the pressure decay in the crossover pressure drop was much faster than in other cases. Even if the data from the air reactor bed was acceptable, the fact that the crossover pressure drop was not stable raised concerns about including this data in the correlation shown in Figure 7. Furthermore, the final pressure drops for both the crossover and the air reactor bed never reached a final steady-state condition. For these reasons, these data were not included in the dataset used to develop the correlation between the crossover pressure drop and the oxygen carrier circulation rate (see Figure 7).

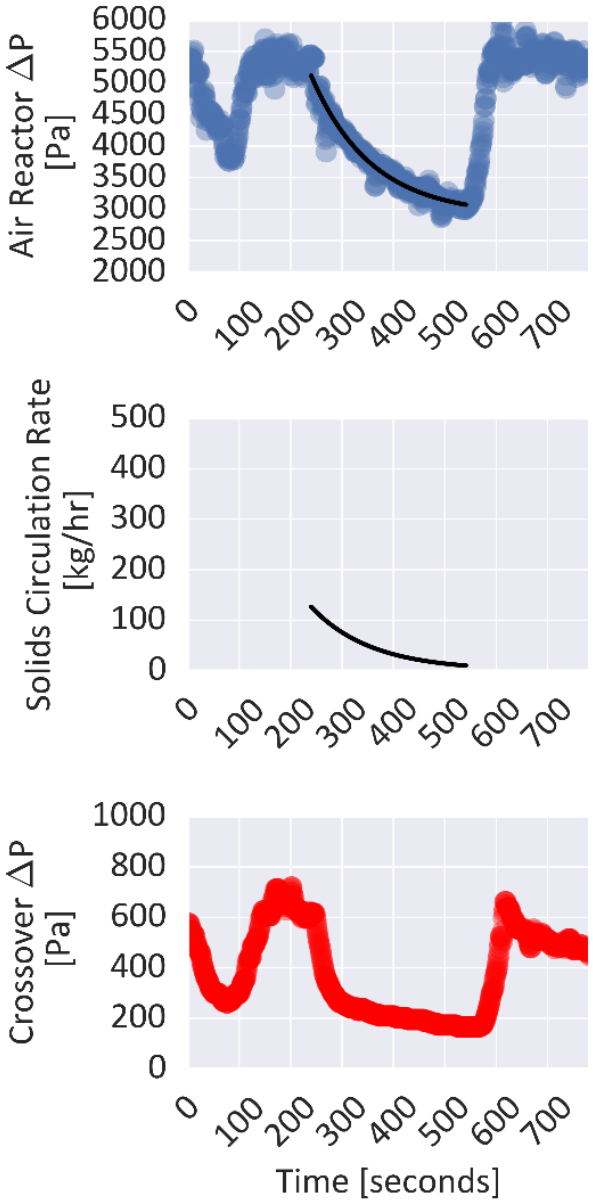

FIGURE 10: UNACCEPTABLE TRANSIENT L-VALVE CUTOFF TEST RESULTS

3.3 Detailed Results

Table 3 lists the time-averaged parameters from the 26 different chemical looping trials in tabular form. Each trial corresponded to one of the green rectangles shown in Figure 8. The longest continuous period of chemical looping combustion was 10 hours (i.e., cumulative period for Trial 1 and Trial 2). For Trials 1-2, the reactor temperatures, emissions, and reactant flows are shown in Figure 11. After approximately 100 minutes, fresh oxygen carrier was added to the air reactor to make-up for oxygen carrier losses. When fresh oxygen carrier materials were added, the air reactor temperature decreases significantly. Natural gas is injected into the air reactor to control the air reactor temperature, and this was particularly important when ambient temperature oxygen carrier material is added to the system. Each of the sudden drops in the air reactor temperature shown in Figure 11 correspond to a batch of fresh oxygen carrier being added to the system. The other reactor temperatures are relatively insensitive to these solids addition events.

After approximately 300 minutes, the first trial ended and the fuel flow to the fuel reactor was approximately doubled (see Figure 11). The average natural gas conversion to carbon dioxide for both trials was 65.0% ± 4.0% (one standard deviation), and did not change significantly as the natural gas flow was doubled. The average carbon closure during the 10 hour period shown in Figure 11 was 98.7% ± 3.6%. As the methane flow to the fuel reactor was doubled, the corresponding fuel flow rate to the air reactor was reduced almost proportionally (see Table 3). The average solids makeup rate during these first two trials was on the average of 2.4 kg/h.

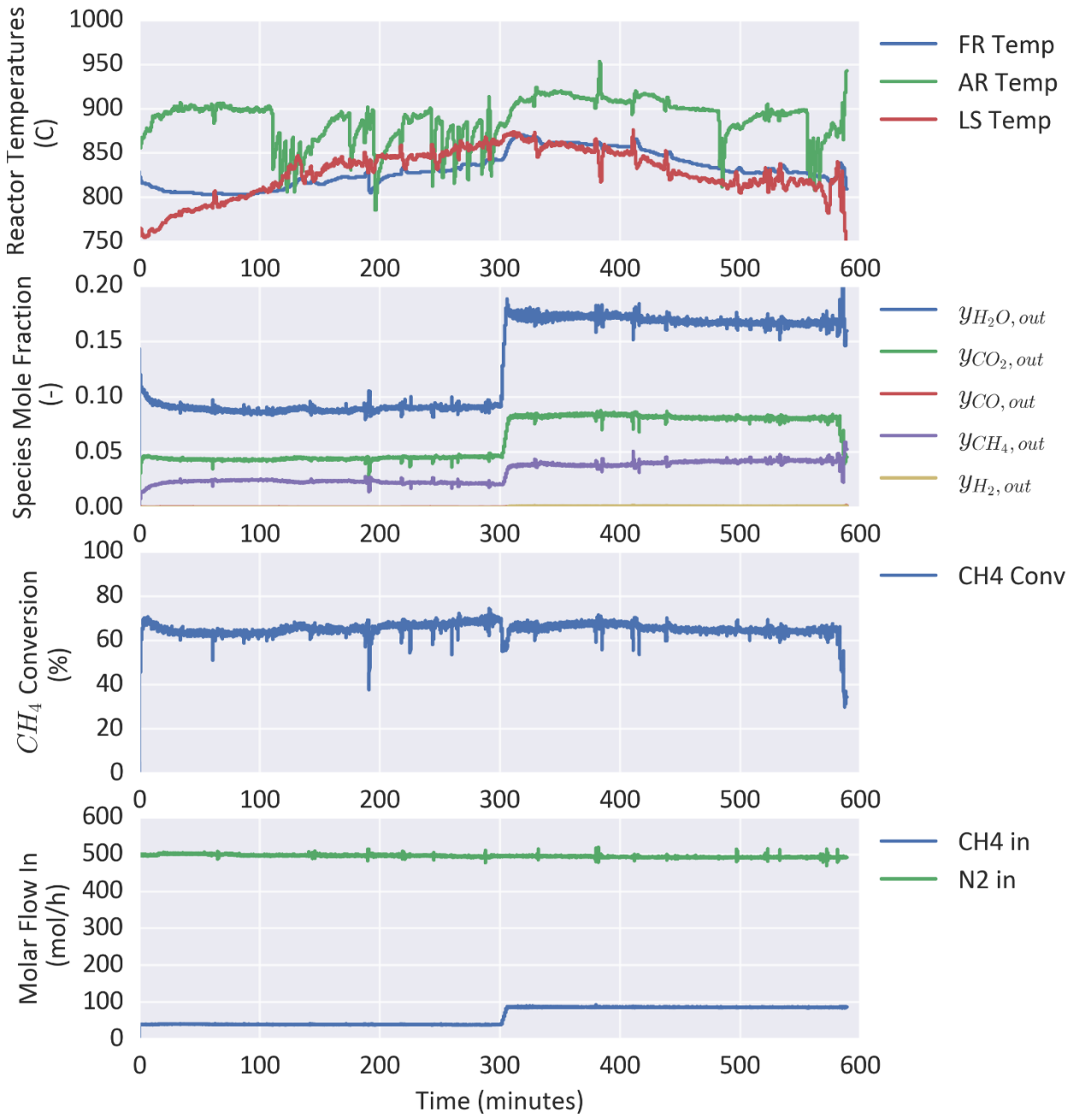

FIGURE 11. FIRST TWO CHEMICAL LOOPING TRIALS SHOWING THE LONG PERIOD OF CHEMICAL LOOPING.

The last four trials of this test campaign (Trials 23-26 as shown in Table 3) were performed without electric preheating of the gases and without combustion of natural gas in the air reactor. A plot of the CLR performance during this time is shown in Figure 12. The fuel flow rate into the system was gradually increased during this time. Approximately 104 minutes of test time was accumulated under these conditions. The fuel reactor temperature ranged from 783-822 °C and the air reactor temperature was ranged from 933-956 °C. For a natural gas feed concentration of around 40-42%, the overall methane conversion ranged from 50-65%, with a significant drop during the last trial. These "auto-thermal" test conditions were achieved near the end of the test campaign, and the decision was made to not add any additional fresh oxygen carrier

material. Therefore, the oxygen carrier inventory was low during these "auto-thermal" test conditions. The gas residence times in the fuel reactor were also very short. The fuel reactor carbon balance during these last trials were lower than the initial trials. While there was no external heat added to the system, the refractory and heater insulators were still at high temperature and some preheating of the gas was still present. So depending on the definition of the "auto-thermal state", more work is required to improve these results.

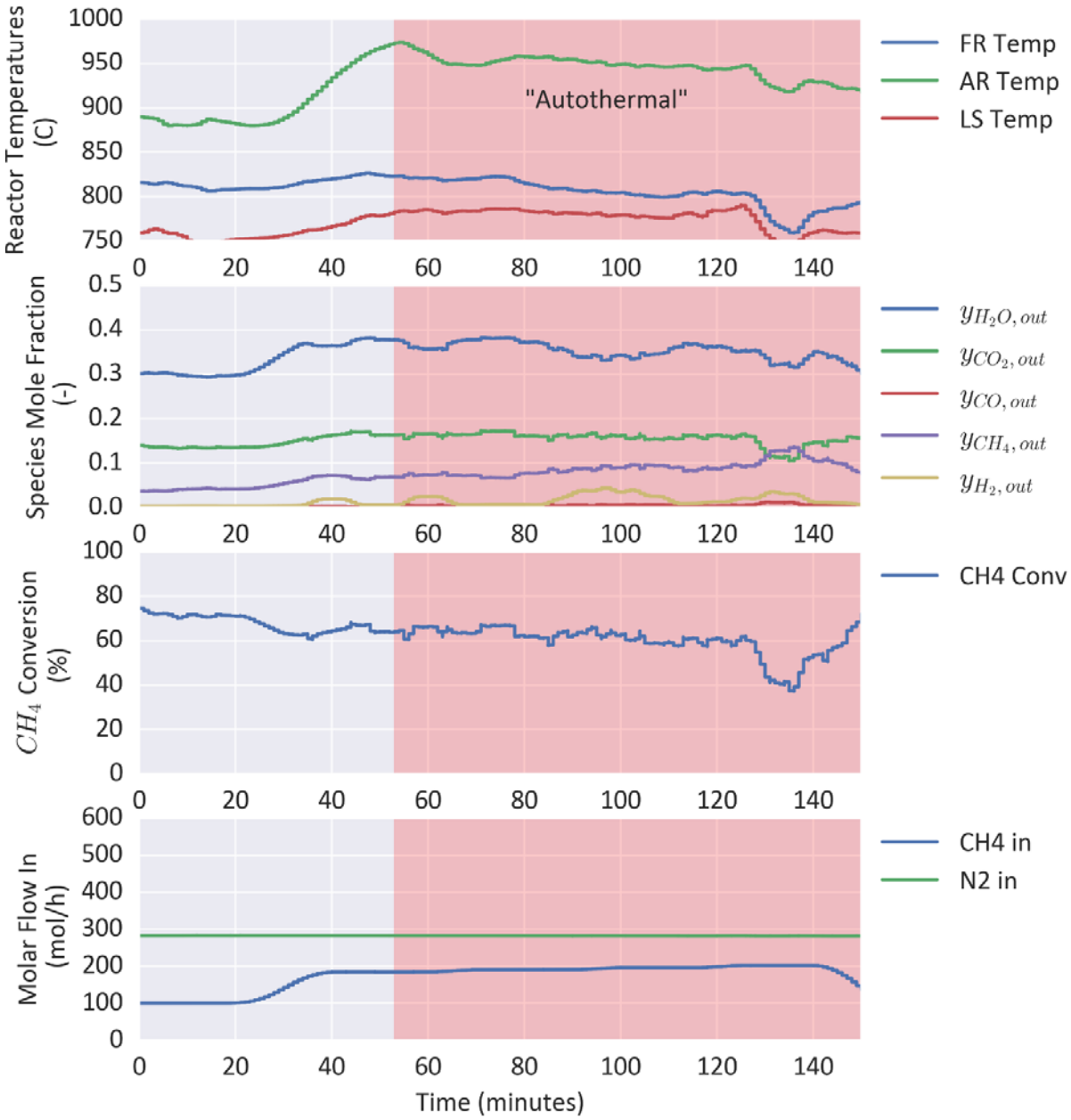

FIGURE 12. PERFORMANCE OF THE CLR WITH NO GAS ELECTRIC PREHEATERS AND NO NATURAL GAS COMBUSTION (TRIALS 23-26 SHADED RED).

TABLE 3. TABULATED AVERAGE RESULTS OF EACH TRIAL PERFORMED DURING THE OPERATION.

	1	2	3	4	5	6
Trial time (min)	301	284	337	25	26	171
Fuel Reactor Temperature (°C)	818	844	812	777	826	794
Air Reactor Temperature (°C)	878	899	893	862	890	889
Fuel Reactor Pressure (kPa)	159	160	158	159	158	158
Inventory (kg)	50	48	49	42	50	47
Gas Residence Time FR (s)	2.24	1.80	1.97	1.37	2.46	1.45
Solids Residence Time FR (s)	720	1901	529	560	1081	741
Fuel Reactor Bed Height (m)	0.61	0.57	0.62	0.50	0.61	0.55
Air Reactor Bed Height (m)	0.52	0.52	0.50	0.48	0.55	0.54
Molar Flow CH4 FR in (mol/h)	39.5	86.3	86.8	55.3	67.5	107.9
Molar Flow N2 FR in (mol/h)	498	493	497	692	388	618
Molar Flow CH4 AR in (mol/h)	1.5	0.8	0.7	1.2	0.7	0.1
Carbon Balance (%)	99.84%	97.70%	97.72%	100.94%	95.82%	99.67%
Methane Conversion to CO2 (%)	65.4%	64.7%	65.2%	54.3%	66.6%	60.6%
Methane Conversion (%)	66.1%	67.6%	67.8%	53.8%	71.3%	61.5%
Oxygen Carrier Utilization (%)	6.8%	37.8%	11.1%	7.5%	18.5%	19.7%
Circulation Rate (kg/h)	153	125	212	153	108	133

	7	8	9	10	11	12
Trial time (min)	32	74	37	185	31	53
Fuel Reactor Temperature (°C)	777	783	795	798	830	801
Air Reactor Temperature (°C)	871	894	919	891	909	897
Fuel Reactor Pressure (kPa)	159	159	159	159	160	160
Inventory (kg)	45	44	38	50	49	51
Gas Residence Time FR (s)	1.38	1.29	1.03	1.78	1.48	2.34
Solids Residence Time FR (s)	651	631	549	702	612	728
Fuel Reactor Bed Height (m)	0.52	0.51	0.42	0.62	0.59	0.63
Air Reactor Bed Height (m)	0.53	0.51	0.48	0.52	0.55	0.54
Molar Flow CH4 FR in (mol/h)	120.9	132.3	144.3	69.1	145.4	27.1
Molar Flow N2 FR in (mol/h)	618	619	619	620	582	518
Molar Flow CH4 AR in (mol/h)	0.0	0.0	0.0	1.1	0.1	1.2
Carbon Balance (%)	99.54%	99.57%	99.28%	100.96%	97.61%	107.09%
Methane Conversion to CO2 (%)	59.4%	61.5%	62.2%	61.0%	62.9%	76.5%
Methane Conversion (%)	60.3%	62.4%	63.4%	60.6%	66.0%	70.0%
Oxygen Carrier Utilization (%)	19.9%	22.7%	24.4%	10.3%	21.5%	5.1%
Circulation Rate (kg/h)	139	140	126	192	168	156

Continued on next page…

Table 3. Continued.

	13	14	15	16	17	18
Trial time (min)	68	79	199	95	38	50
Fuel Reactor Temperature (°C)	797	823	807	777	781	759
Air Reactor Temperature (°C)	905	912	921	906	898	900
Fuel Reactor Pressure (kPa)	159	159	159	158	159	159
Inventory (kg)	48	48	46	40	41	35
Gas Residence Time FR (s)	2.16	1.87	1.92	1.23	1.33	1.31
Solids Residence Time FR (s)	708	753	835	1181	704	801
Fuel Reactor Bed Height (m)	0.58	0.57	0.56	0.46	0.47	0.35
Air Reactor Bed Height (m)	0.53	0.54	0.52	0.48	0.49	0.46
Molar Flow CH4 FR in (mol/h)	27.5	108.4	81.9	108.3	35.3	54.0
Molar Flow N2 FR in (mol/h)	520	437	465	621	693	491
Molar Flow CH4 AR in (mol/h)	1.1	0.3	0.5	0.1	1.0	0.5
Carbon Balance (%)	98.05%	96.79%	96.24%	97.73%	98.74%	96.24%
Methane Conversion to CO2 (%)	65.5%	67.6%	64.7%	57.3%	53.8%	52.7%
Methane Conversion (%)	67.8%	71.3%	69.0%	60.1%	55.5%	56.9%
Oxygen Carrier Utilization (%)	4.9%	22.2%	18.2%	35.9%	6.4%	16.3%
Circulation Rate (kg/h)	145	142	126	72	127	79

	19	20	21	22	23	24
Trial time (min)	33	72	19	56	29	29
Fuel Reactor Temperature (°C)	776	751	798	814	822	814
Air Reactor Temperature (°C)	895	899	947	900	956	953
Fuel Reactor Pressure (kPa)	159	160	161	161	161	161
Inventory (kg)	37	35	35	36	34	34
Gas Residence Time FR (s)	1.43	0.98	1.41	1.57	1.13	1.12
Solids Residence Time FR (s)	530	382	353	338	294	313
Fuel Reactor Bed Height (m)	0.38	0.34	0.33	0.34	0.32	0.32
Air Reactor Bed Height (m)	0.49	0.50	0.49	0.50	0.48	0.47
Molar Flow CH4 FR in (mol/h)	54.1	72.7	173.4	100.1	185.1	190.8
Molar Flow N2 FR in (mol/h)	492	657	209	283	283	282
Molar Flow CH4 AR in (mol/h)	0.7	0.9	0.0	0.0	0.0	0.0
Carbon Balance (%)	94.97%	97.59%	86.05%	94.64%	93.75%	94.33%
Methane Conversion to CO2 (%)	50.5%	33.9%	58.9%	74.6%	65.3%	63.6%
Methane Conversion (%)	56.0%	37.0%	73.6%	80.2%	72.5%	70.5%
Oxygen Carrier Utilization (%)	8.8%	6.5%	27.1%	16.8%	25.4%	27.2%
Circulation Rate (kg/h)	127	156	165	179	194	182

Continued on next page…

Table 3. Continued.

	25	26
Trial time (min)	24	22
Fuel Reactor Temperature (°C)	802	783
Air Reactor Temperature (°C)	946	932
Fuel Reactor Pressure (kPa)	161	160
Inventory (kg)	33	31
Gas Residence Time FR (s)	1.11	1.02
Solids Residence Time FR (s)	345	355
Fuel Reactor Bed Height (m)	0.32	0.28
Air Reactor Bed Height (m)	0.45	0.44
Molar Flow CH4 FR in (mol/h)	196.7	202.3
Molar Flow N2 FR in (mol/h)	282	282
Molar Flow CH4 AR in (mol/h)	0.0	0.0
Carbon Balance (%)	95.37%	91.83%
Methane Conversion to CO2 (%)	59.8%	50.7%
Methane Conversion (%)	66.2%	61.3%
Oxygen Carrier Utilization (%)	29.0%	32.0%
Circulation Rate (kg/h)	171	146

3.4 Parametric Test Results

Because the size of the unit is relatively large, it is challenging to extract precise kinetic data from the operation of the unit. Nevertheless, plotting changes in the operating parameters, such as the solids flow rate, fuel gas residence time, etc. on the unit performance, namely the fuel conversion, can be performed to gleam general trends. An ordinary least squares analysis of the natural gas conversion to carbon dioxide was performed using statsmodels in the programming language Python. The independent variables in the analysis include the fuel reactor temperature, fuel reactor pressure, natural gas feed concentration, gas residence time, and solids residence time in the fuel reactor. If it is assumed there is no interaction between the parameters, the regression model is

$$\hat{X}_{\mathrm{CH_4 \rightarrow CO_2}} = \hat{\beta}_0 + \hat{\beta}_1 x_{\mathrm{Temp}} + \hat{\beta}_2 x_{\mathrm{Press}} + \hat{\beta}_3 x_{\mathrm{Conc}} + \hat{\beta}_4 x_{\tau_{\mathrm{g,FR}}} + \hat{\beta} x_{\tau_{\mathrm{OC,FR}}} \quad (24)$$

Where x_i are the coded variables of temperature, pressure, concentration, gas residence time, and solids residence time in the fuel reactor. The independent variables are coded such that the maximum value is positive one, while the minimum value is negative one. This allows the size of the coefficients to reveal the strength of the effect on the methane conversion.

For the range of conditions investigated, the variable that had the greatest effect on the fuel conversion performance was the fuel reactor temperature. As can be seen from Table 3, the fuel reactor temperature ranged from 750-845°C, and this effect was almost twice as large as the next most significant factor. The second-most significant parameter was the gas residence time which varied from approximately 1.0-2.5 seconds. The gas residence time in the fuel reactor is mainly a function of bed height (and solids inventory), temperature, and gas flow rate. As the gas spends more time in the fluidized bed, the natural gas is more likely to convert. This suggests that an improved design for the fuel reactor should have a greater solids height to allow for more conversion of the gas. However, there is a limit on the solids bed height, since small

bubbles tend to coalesce and form larger bubbles with increasing height of the fuel reactor. The larger bubbles can reduce the fuel conversion because the unconverted gas bypasses the emulsion phase. Other options could be used to overcome this issue, such as adding baffles that break-up the larger bubbles.

Figure 13 and Figure 14 show the natural gas conversion to CO_2 for each of the 26 trials as a function of fuel reactor temperature and fuel reactor gas residence time, respectively. In Figure 13, the symbol color corresponds to the average gas residence time in the fuel reactor. In Figure 14, the symbols are colored based on the averaged fuel reactor bed temperature. In spite of the large number of variables associated with a circulating CLC system, the data from this test suggests that the fuel reactor temperature had the most significant effect on the fuel conversion.

TABLE 4. ORDINARY LEAST SQUARES ANALYSIS OF TRIALS ON METHANE CONVERSION TO CO_2.

	Term	Coefficient	Standard Error	t-Statistic	P>|t|
Intercept	$\hat{\beta}_0$	0.6038	0.030	20.312	0.000
Temperature	$\hat{\beta}_1$	0.1085	0.038	2.876	0.009
Pressure	$\hat{\beta}_2$	-0.0288	0.029	-0.998	0.330
Concentration	$\hat{\beta}_3$	0.0188	0.033	0.577	0.570
Gas Residence Time	$\hat{\beta}_4$	0.0562	0.031	1.834	0.082
Solid Residence Time	$\hat{\beta}_5$	-0.0388	0.034	-1.128	0.273

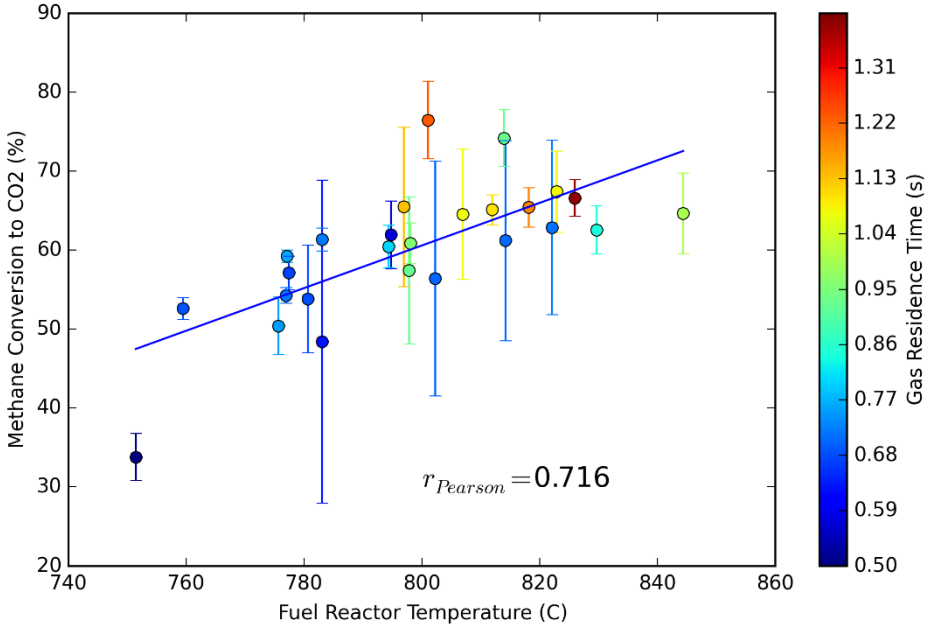

FIGURE 13. EFFECT OF FUEL REACTOR TEMPERATURE ON THE METHANE CONVERSION TO CARBON DIOXIDE.

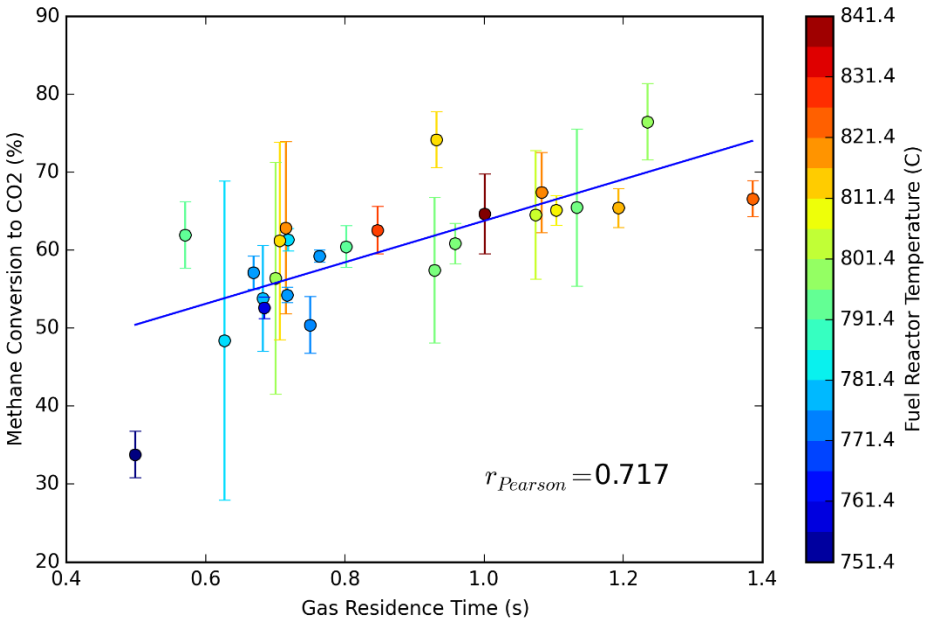

FIGURE 14. EFFECT OF GAS RESIDENCE TIME ON THE METHANE CONVERSION TO CARBON DIOXIDE.

3.5 Oxygen Carrier Losses And Make-Up Rates

As previously described, one of the critical issues for chemical looping combustion systems is the cost associated with the oxygen carrier material. More specifically, the material cost required to maintain the oxygen carrier inventory and the material cost to offset oxygen carrier losses has a significant impact on the plant operating cost. Oxygen carrier losses could be due to attrition, cyclone performance, degradation in reactivity, or other operational conditions. In this section, the oxygen carrier losses recorded during each of the chemical looping combustion trials will be discussed.

Prior to the hot test campaign, some abrasion-type attrition was observed with this oxygen carrier material at room temperature. This has been described in Section 2.2. During the hot test campaign, oxygen carrier materials were collected from the downstream cyclones and weighed (see Figure 2). Fine materials that passed through these secondary cyclones were also collected on downstream filters. The fines collected on the barrier filters were not weighed, since the weight of this material was small. In many cases, fines became embedded into the filter elements and were not weighed. During this test campaign, the filter elements required frequent cleaning, so there was some evidence to suggest that abrasion-type attrition continued throughout the hot test campaign. The filter element on the air reactor vent line required the most frequent maintenance, and the amount of oxygen carrier loss from this process stream was significantly larger than the exhaust streams.

Most of the oxygen carrier material that left the main process was captured by the secondary cyclones. In Table 5, the average oxygen carrier loss rate through each of these secondary cyclones has been listed as a function of the test period. These data show the fuel reactor vent line exhibited the lowest oxygen carrier loss rates, followed by the seal pot exhaust, and the air reactor exhaust. Although the seal pot operated at a lower gas velocity, more oxygen carrier was lost. One potential reason for the higher material loss rate may be due to the fact that the seal pot was very short, and the outlet from the seal pot was much closer to the

bed material compared to the fuel reactor. The largest rate of solids loss was collected in the secondary cyclone on the air reactor exhaust line.

Based on empirical relations, the primary cyclone efficiency has been calculated to be 98.4%, with a 50% particle cutoff size of 3 μm. Therefore, a small fraction of oxygen carrier material losses were expected. Using the calculated cyclone efficiency and the measured oxygen carrier circulation rate, oxygen carrier loss rates based on the theoretical cyclone efficiency from the air reactor vent line ranged from 1.1 to 3.3 kg/h. This solids loss rate based on the theoretical cyclone efficiency estimate was typically larger than the measured solids loss rate from the secondary cyclone. This may be due to a modification that was made to the primary cyclone vortex finder. Instead of a conventional vortex finder, the bottom of the vortex finder was closed and slots were cut into the sides of the vortex finder. This modification may have increased the cyclone efficiency. Additionally, very fine particles bypass the secondary cyclone and were collected in the downstream filters. The mass of fines captured in the downstream filter elements was not measured, as described above. Given all the uncertainties, the measured solids loss rates from the primary cyclone and the values approximated based on the theoretical cyclone efficiency were in reasonable agreement.

For the entire test campaign, the average total oxygen carrier loss rate was on the order of 1.4 kg/hr, and approximately 50% of those losses originated from the air reactor, or primary cyclone, exhaust. These results are very process specific and do not necessarily reflect the type of losses that would be expected in a larger scale system. In a larger scale system, the solids from these secondary cyclones would be recirculated back into the process. However, for the purposes of this test campaign, only fresh oxygen carrier material was added to the system.

If fresh oxygen carrier materials were added to the system at approximately the same rate that solids were lost (i.e. approximately 1.4 kg/hr), then it is important to determine whether the fresh oxygen carrier make-up rate was large relative to the total inventory. If the fresh material make-up rate was too large, then the measured carrier performance could have been biased toward the performance of the fresh oxygen carrier material. For the measured oxygen carrier loss rate, an average time required to replace the oxygen carrier inventory for each test trial has been listed in Table 5. A simple ratio of the oxygen carrier inventory in the system to the average carrier loss rate from all three secondary cyclones has been tabulated in Table 5 as "hours to replace entire inventory". In most of the trials for this test campaign, this time scale was significantly longer than the duration of the chemical looping combustion testing. Therefore, the results were not significantly affected by the addition of fresh oxygen carrier material. In the future, recycling the material from these secondary cyclone drains will be considered.

In an attempt to identify another performance metric to characterize the oxygen carrier performance, Table 5 also lists the average number of cycles that an oxygen carrier material completed per specific test trial. This metric was based on the solids inventory in the system; the oxygen carrier circulation rate; and the test trial duration. All of the trials had a solids circulation rate that was high enough, or a test duration that was long enough, to achieve one or more complete cycles on the oxygen carrier material. The largest number of cycles was achieved in test Trial 3 which was about five hours in duration and had an oxygen carrier circulation of approximately 200 kg/hr. In the future, the test plans will target larger numbers of cycles per trial.

Although the carbon mass closure was very good for most of the test periods, the solid oxygen carrier mass closure was more difficult. From the estimate of the solids inventory in the vessel and the tabulated solids added and collected from the system, the solids accounting deficit can be determined. The following formula has been used for the missing solids calculation at any time during the run:

$$m_{\text{missing}} = m_{\text{added}} - m_{\text{out,AR}} - m_{\text{out,FR}} - m_{\text{out,LS}} - m_{\text{inv}} \quad (23)$$

Where m_{added} was the cumulative weight solids added to the system over the entire run, and $m_{\text{out},i}$ were the cumulative weights of solids collected from each secondary cyclone. The solids inventory in the system, m_{inv}, was estimated from the reactor bed pressure drops. As can be seen from Figure **15**, the missing solids were relatively low until the first chemical looping combustion period started. Then a system upset occurred on the morning of July 12. The missing solids increased to above 30 kg. During this upset, a significant amount of solids were collected from the filter banks and the weight was not recorded. During this upset condition, some solids were also collected in the outlet piping. More work is required to achieve better closure on the solids mass balance.

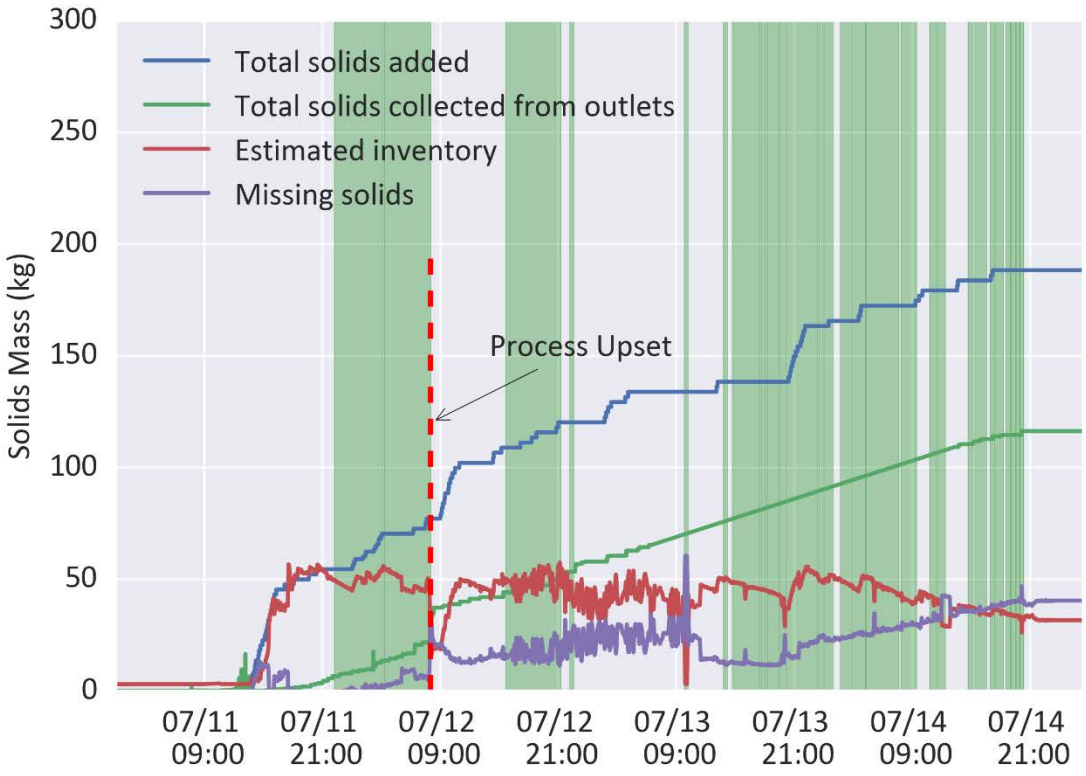

FIGURE 15. SOLIDS MAKEUP AND SOLIDS COLLECTED FROM SECONDARY CYCLONES DURING THE RUN.

TABLE 5. RATE OF CARRIER LOSSES FROM THE UNIT.

	Air Reactor Mass Collected	Fuel Reactor Mass Collected	Seal Pot Mass Collected	Total	Inventory	Hours to replace entire bed	No. of Cycles
	kg/h	kg/h	kg/h	kg/h	kg	h	-
1	0.6	0.0	0.7	1.4	50	35	15.5
2	2.4	0.1	0.9	3.5	48	14	12.4

	Air Reactor Mass Collected	Fuel Reactor Mass Collected	Seal Pot Mass Collected	Total	Inventory	Hours to replace entire bed	No. of Cycles
3	0.6	0.2	0.5	1.3	49	37	24.3
4	0.0	0.0	0.0	0.0	42		1.5
5	0.7	0.2	0.5	1.4	50	35	0.9
6	0.7	0.2	0.5	1.4	47	33	8.1
7	0.7	0.2	0.5	1.4	45	32	1.6
8	0.7	0.2	0.5	1.4	44	31	4.0
9	0.7	0.2	0.5	1.4	38	27	2.0
10	0.7	0.2	0.5	1.4	50	35	11.9
11	0.7	0.2	0.5	1.4	49	34	1.8
12	0.7	0.2	0.5	1.4	51	36	2.7
13	0.7	0.2	0.5	1.4	48	34	3.4
14	0.7	0.2	0.5	1.4	48	33	3.9
15	0.7	0.2	0.5	1.4	46	33	9.0
16	0.7	0.2	0.5	1.4	40	28	2.8
17	0.7	0.2	0.5	1.4	41	29	2.0
18	0.7	0.2	0.5	1.4	35	24	1.9
19	0.7	0.0	0.6	1.3	37	30	1.8
20	0.4	0.1	0.3	0.8	35	43	5.3
21	2.5	0.5	1.0	4.0	35	9	1.5
22	0.4	0.0	0.3	0.7	36	54	4.7
23	0.0	0.0	0.0	0.0	34		2.7
24	0.0	0.0	0.0	0.0	34		2.6
25	0.0	0.0	0.0	0.0	33		2.1
26	2.1	1.2	1.3	4.6	31	7	1.7

3.6 Assessment Of Oxygen Carrier Make-Up Costs

The last metric discussed in this section is an oxygen carrier make-up cost that is normalized by the amount of heat released in the fuel reactor. Based on previous studies,[5] an important goal is to achieve a normalized oxygen carrier makeup cost of less than $\$5/\text{MW}_{\text{th}}\text{-hr}$. By achieving this important performance milestone, a coal-fired chemical looping combustion technology could meet and possibly exceed the DOE 2035 Goals.

The following expression has been used to calculate this normalized oxygen carrier makeup cost.

$$\text{Makeup Cost}\left(\frac{\$}{\text{MW}_{\text{th}}\text{-hr}}\right) = \frac{W_{\text{OC}}\dot{m}_{\text{loss}}(1-\alpha)}{\dot{N}_{\text{CH}_4,\text{in}}X_{\text{CH}_4\rightarrow\text{CO}_2}HHV_{\text{CH}_4}} \times \left(3.6\times10^6\frac{\text{kJ}}{\text{MWh}}\right) \quad (26)$$

Where W_{OC} is the unit cost of the oxygen carrier ($/kg), $\dot{m}_{\text{loss}}$ is the oxygen carrier loss rate from the system, α is the fraction of elutriated carrier that is recycled back into the system, and HHV_{CH_4} is the higher heating value of methane (889 kJ/mol). Note that methane has been used to approximate the properties of the

natural gas. The fuel conversion, $X_{CH_4 \rightarrow CO_2}$, is also incorporated into this expression to account for the reactivity of the oxygen carrier material and the performance observed in this test campaign.

Although many of the parameters described in Equation 26 were related to this specific test apparatus, some semi-quantitative metric, or bench-mark, was sought to provide a baseline comparison for future oxygen carrier material tests. Many of the parameters that influence this performance metric are process dependent, so extrapolation of these results to larger scale applications is not recommended.

Although this oxygen carrier material was manufactured using a wet granulation method which has the potential to achieve lower cost products, the unit cost of the oxygen carrier material will be treated as an independent parameter in the following discussion. Furthermore, the fraction of oxygen carrier material that can be recycled back into the process has been treated as an independent parameter. When the actual test data were plotted below, a recycle rate of 90% was assumed. This 90% recycle rate means that 90% of the oxygen carrier collected from the secondary cyclones during this test campaign could be recycled into the process without impacting the overall performance.

Figure 16 shows the cost of oxygen carrier makeup as a function of oxygen carrier cost. The red data points represent the range of oxygen carrier makeup rate measured from this specific test apparatus. All of the test conditions have been plotted for two different oxygen carrier material costs. The dotted horizontal line indicates a goal for oxygen carrier makeup cost that would enable a chemical looping combustion system to meet, and possibly exceed the DOE 2035 Goals. Figure 16 shows the range of oxygen carrier losses observed during this test campaign. Although this was a fairly wide variation in the experimental observations, a wide range of process conditions were also investigated. In short, the oxygen carrier makeup costs could be improved from a process perspective (i.e, by reducing the loss rates), but the cost of the oxygen carrier material is also an important parameter.

As previously mentioned, the theoretical primary cyclone efficiency was approximately 99% and the observed rate of oxygen carrier collected from the secondary cyclones were consistent with this cyclone efficiency. In Figure 16, the colored lines represent different recycle rates for the solids that were collected from the secondary cyclones. For example, if 90% of the oxygen carrier collected from the secondary cyclones during this campaign could be recirculated into the process, then the oxygen carrier loss rate would have been approximately 0.1% of the oxygen carrier circulation rate. The experimentally measured rates of oxygen carrier collected from the secondary cyclones have been plotted in Figure 16 assuming 90% recycle rate. The contours of constant recycle rate suggest that a practical pathway to the goal must include reductions in the oxygen carrier cost and reductions in the oxygen carrier losses.

The oxygen carrier circulation rates for this test campaign were significantly lower relative to other tests performed using hematite. Furthermore, it was observed that these lower oxygen carrier circulation rates did not significantly impact the fuel conversion to CO_2. The oxygen carrier utilization estimated in Table 2 was also low for many of the test conditions. Therefore, it is plausible that the oxygen transport capacity of this material was not fully utilized during these tests and it may be possible to further reduce the oxygen carrier circulation rate. Lower circulation rates are expected to result in lower oxygen carrier losses.

Another approach to reduce the normalized oxygen carrier make-up rate in Figure 16 is to achieve better fuel conversion to CO_2. All of these options will be explored in the future to progress towards the research goal of \$5/MW_{th}-hr.

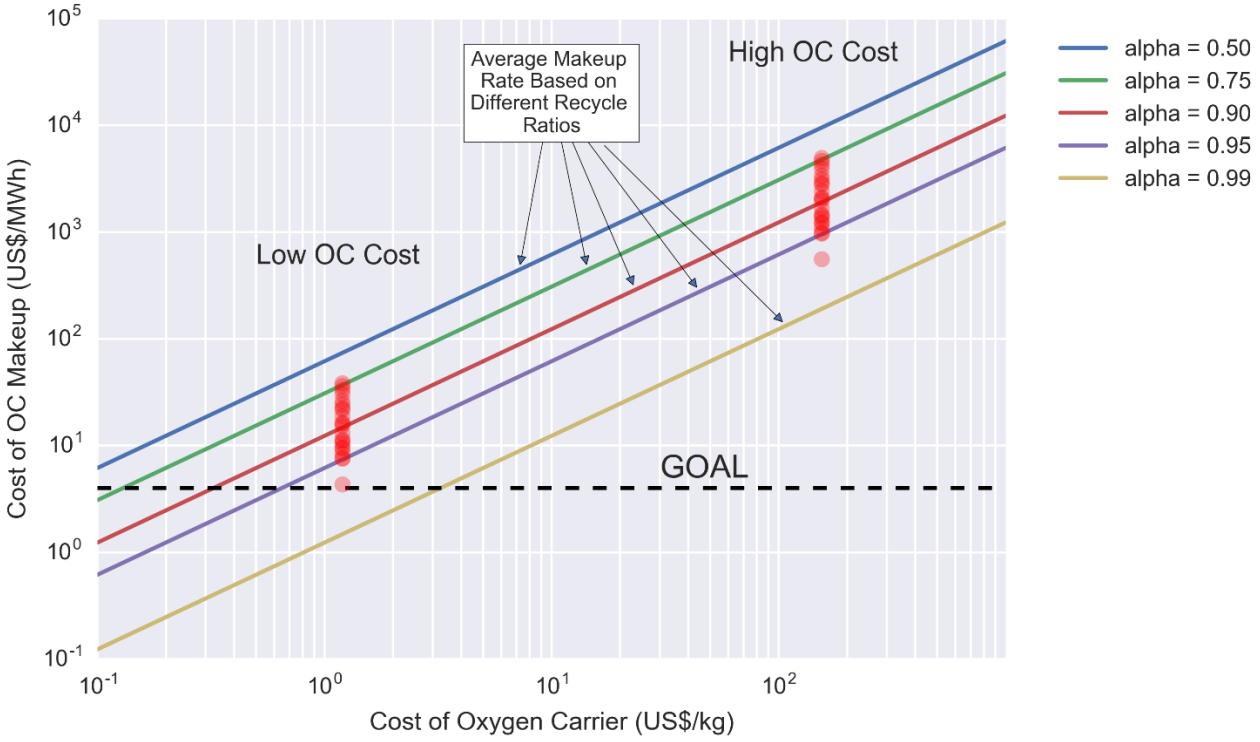

FIGURE 16. SENSITIVITY OF OXYGEN CARRIER MAKEUP COST TO THE COST OF OXYGEN CARRIER AND RECYCLE RATIO (ALPHA) BASED ON OPERATIONAL DATA.

4. CONCLUSIONS

This report described the first proof-of-concept test for NETL's second generation Cu/Fe/alumina oxygen carrier material. This test was performed using NETL's 50kW$_{th}$ circulating Chemical Looping Reactor (CLR) test facility. Although this test facility was relatively small, the operating environment had many of the key characteristics of a realistic CLC environment. The test campaign started on July 10, 2016 and continued for more than five days. During this test campaign, the following highlights were achieved:

- The oxygen carrier materials were circulated for approximately 4.3 days in the target temperature range (700-850°C).
- Twenty-six different CLC test periods were completed and a total of approximately 40 hours of chemical looping combustion testing was accumulated. The average fuel reactor temperatures ranged from 760-815°C for these test periods, and the average air reactor temperature ranged from 840-915°C. The fuel conversion from natural gas to CO_2 ranged from 50-80%.
- Nine test periods were completed with no natural gas combustion in the air reactor to augment the heat release from the oxygen carrier material. Approximately 5.3 hours of test time was accumulated without natural gas augmented heating.
- Four test periods (Trials 23-26 as shown in Table 3) were performed without electric preheating of the gases and without combustion of natural gas in the air reactor. Approximately 1.6 hours of continuous operation was achieved with no gas preheat and no natural gas augmented heating. The average fuel reactor temperature ranged from 780-825°C during these test periods and the air reactor temperature ranged from 930-960°C. The natural gas to CO_2 conversion ranged from 50-65%.

The oxygen carrier circulation rate was an important parameter for understanding the fundamental oxygen carrier performance in this test campaign. The oxidant-to-fuel ratio in the fuel reactor was set by the solids circulation rate. This report described a transient approach to correlate the solids mass flow rate with the pressure drop across the horizontal transport region between the top of the riser and the entrance to the cyclone (i.e., cross-over region). The average oxygen carrier circulation rate for each CLC test period was calculated and tabulated in Table 3. These circulation rates were significantly lower than previous tests using a natural hematite oxygen carrier. The oxygen carrier circulation rates during this test campaign ranged from 72-212 kg/hr.

In spite of the lower oxygen carrier circulation rates and lower fuel reactor temperatures, the natural gas to CO_2 conversion was significantly higher than previous tests using hematite. For NETL's second generation Cu/Fe/alumina material, the fuel to CO_2 conversion ranged from 50-80% and the carbon mass closure was generally within 5%. In an attempt to understand the effects of several different operating parameters, a simple multi-variable regression model was fit to the fuel-to-CO_2 conversion. Five different parameters were included in the linear (main effects only) model. The fuel reactor temperature effect on the fuel to CO_2 conversion was the most significant factor. Factors such as the pressure, fuel inlet concentration, and solids residence time did not have a statistically significant effect on the fuel to CO_2 conversion over the range of conditions investigated. Although this finding suggests that the lower oxygen carrier circulation rates were not limiting the fuel to CO_2 conversion, more work is warranted.

Oxygen carrier losses were also collected from each of the three exhaust lines (i.e., air reactor, fuel reactor, and seal pot). The oxygen carrier losses from the air reactor's primary cyclone were higher than the other two exhaust lines by almost a factor of two. The measured oxygen carrier loss rates were used to estimate a normalized oxygen carrier make-up cost ($/MW$_{th}$-hr) as shown in Figure 16. Based on the assumptions and the data collected from this test campaign, the pathway to achieve a oxygen carrier make-up cost performance goal of less than $5/ MW$_{th}$-hr should include reductions in oxygen carrier cost and reductions in the oxygen carrier loss rate. This particular oxygen carrier material has shown significant promise for

reducing the required solids circulation rates and still achieving relatively high fuel-to-CO_2 conversion. The analysis of this data has suggested additional improvements. Furthermore, oxygen carrier materials with a high oxygen transport capacity should be evaluated as a potential pathway to achieve the DOE 2035 Goals.

It has been estimated that the system operated for over 130 oxidation/reduction cycles, but not all of the oxygen carrier material was exposed to 130 cycles. Fresh oxygen carrier material was continuously added to maintain a constant solids inventory, so more work is required to get better estimates of the oxygen carrier lifetime. The oxygen carrier degradation and life is a critical parameter in the technoeconomic analysis of chemical looping systems for power generation. In the future, the oxygen carrier materials collected from the secondary cyclones may be screened and recycled to get better estimates on the effects of recycle and oxygen carrier durability. Future work may also include the addition of steam to enhance the fuel conversion, and longer duration tests under “auto-thermal” operation.

5. REFERENCES

1. U.S. Environmental Protection Agency Sources of Greenhouse Gas Emissions. https://www3.epa.gov/climatechange/ghgemissions/sources/electricity.html (accessed 2016-05-06).

2. U.S. Energy Information Agency Annual Energy Outlook 2016. http://www.eia.gov/forecasts/aeo/section_elecgeneration.cfm (accessed 2016-10-03).

3. Gilliland, E.; Lewis, W. Production of Pure Carbon Dioxide. 2,665,971, May 12, 1954.

4. Adanez, J.; Abad, A.; Garcia-Labiano, F.; Gayan, P.; de Diego, L. F., Progress in Chemical-Looping Combustion and Reforming technologies. *Progress in Energy and Combustion Science* **2012**, *38* (2), 215-282.

5. National Energy Technology Laboratory, Guidance for NETL's Oxy-combustion R&D Program: Chemical Looping Combustion Reference Plant Designs and Sensitivity Studies. 2014.

6. Siriwardane, R.; Tian, H.; Simonyi, T.; Poston, J., Synergetic effects of mixed copper–iron oxides oxygen carriers in chemical looping combustion. *Fuel* **2013**, *108*, 319-333.

7. Siriwardane, R.; Tian, H.; Miller, D.; Richards, G., Fluidized bed testing of commercially prepared MgO-promoted hematite and CuO–Fe2O3 mixed metal oxide oxygen carriers for methane and coal chemical looping combustion. *Applied Energy* **2015**, *157*, 348-357.

8. Monazam, E. R.; Breault, R. W.; Tian, H.; Siriwardane, R., Reaction Kinetics of Mixed CuO–Fe2O3with Methane as Oxygen Carriers for Chemical Looping Combustion. *Industrial & Engineering Chemistry Research* **2015**, *54* (48), 11966-11974.

9. Kunii, D.; Levenspiel, O., *Fluidization Engineering*. 2nd ed.; Butterworth Heinemann: Boston, 1991.

10. International, A., Standard Test Method for Determination of Attrition of FCC Catalysts by Air Jets. 2011; Vol. D5757-11, p 3.

11. Werther, J.; Reppenhagen, J., *Attrition in fluidized beds and pneumatic conveying lines*. William Andrew Publishing: Fluidization, solids handling and processing, 1999.

6. APPENDIX

Table A1. Detailed tabulated results of the trials during the operation.

	1	2	3	4	5	6
Trial time (min)	301	284	337	25	26	171
Fuel Reactor Temperature (°C)	818	844	812	777	826	794
Air Reactor Temperature (°C)	878	899	893	862	890	889
Fuel Reactor Pressure (kPa)	159	160	158	159	158	158
Inventory (kg)	50	48	49	42	50	47
Gas Residence Time FR (s)	2.24	1.80	1.97	1.37	2.46	1.45
Solids Residence Time FR (s)	720	1901	529	560	1081	741
Fuel Reactor Bed Height (m)	0.61	0.57	0.62	0.50	0.61	0.55
Air Reactor Bed Height (m)	0.52	0.52	0.50	0.48	0.55	0.54
Molar Flow CH4 FR in (mol/h)	39.5	86.3	86.8	55.3	67.5	107.9
Molar Flow N2 FR in (mol/h)	498	493	497	692	388	618
Molar Flow CO2 FR out (mol/h)	26	56	57	30	45	65
Molar Flow CO FR out (mol/h)	0	0	0	0	0	1
Molar Flow CH4 FR out (mol/h)	13	28	28	26	19	42
Molar Flow H2 FR out (mol/h)	0	1	1	0	0	1
Molar Flow N2 FR out (mol/h)	492	489	490	685	381	611
Molar Flow H2O FR out (mol/h)	52	117	118	60	96	133
Molar Flow CH4 AR in (mol/h)	1.5	0.8	0.7	1.2	0.7	0.1
Molar Flow Air AR in (mol/h)	2239	2206	2138	2218	1830	1798
Molar Flow CO2 AR out (mol/h)	102	58	53	81	47	10
Molar Flow N2 AR out (mol/h)	1862	1865	1816	1858	1483	1484
Molar Flow O2 AR out (mol/h)	200	222	226	228	228	215
Molar Flow H2O AR out (mol/h)	176	97	90	141	83	14
Carbon Balance (%)	99.84%	97.70%	97.72%	100.94%	95.82%	99.67%
Methane Conversion to CO2 (%)	65.4%	64.7%	65.2%	54.3%	66.6%	60.6%
Methane Conversion (%)	66.1%	67.6%	67.8%	53.8%	71.3%	61.5%
Oxygen Carrier Utilization (%)	6.8%	37.8%	11.1%	7.5%	18.5%	19.7%
Circulation Rate (kg/h)	153	125	212	153	108	133
Average FR Velocity In (m/s)	0.26	0.29	0.29	0.35	0.23	0.35
Average FR Velocity Out (m/s)	0.28	0.34	0.34	0.38	0.27	0.41
Average FR Velocity (m/s)	0.27	0.32	0.31	0.36	0.25	0.38
Average AR Velocity (m/s)	0.52	0.53	0.53	0.52	0.54	0.54
Riser Gas Velocity (m/s)	11.8	11.8	11.4	11.5	9.8	9.6

Continued on next page…

Table 3. Continued.

	7	8	9	10	11	12
Trial time (min)	32	74	37	185	31	53
Fuel Reactor Temperature (°C)	777	783	795	798	830	801
Air Reactor Temperature (°C)	871	894	919	891	909	897
Fuel Reactor Pressure (kPa)	159	159	159	159	160	160
Inventory (kg)	45	44	38	50	49	51
Gas Residence Time FR (s)	1.38	1.29	1.03	1.78	1.48	2.34
Solids Residence Time FR (s)	651	631	549	702	612	728
Fuel Reactor Bed Height (m)	0.52	0.51	0.42	0.62	0.59	0.63
Air Reactor Bed Height (m)	0.53	0.51	0.48	0.52	0.55	0.54
Molar Flow CH4 FR in (mol/h)	120.9	132.3	144.3	69.1	145.4	27.1
Molar Flow N2 FR in (mol/h)	618	619	619	620	582	518
Molar Flow CO2 FR out (mol/h)	72	81	90	42	91	21
Molar Flow CO FR out (mol/h)	1	1	1	0	1	0
Molar Flow CH4 FR out (mol/h)	48	50	53	27	50	8
Molar Flow H2 FR out (mol/h)	1	2	2	1	3	0
Molar Flow N2 FR out (mol/h)	611	612	612	613	575	512
Molar Flow H2O FR out (mol/h)	146	165	183	84	192	38
Molar Flow CH4 AR in (mol/h)	0.0	0.0	0.0	1.1	0.1	1.2
Molar Flow Air AR in (mol/h)	1791	1786	1784	1845	1784	1852
Molar Flow CO2 AR out (mol/h)	1	1	2	77	9	80
Molar Flow N2 AR out (mol/h)	1485	1481	1479	1538	1497	1498
Molar Flow O2 AR out (mol/h)	222	199	182	132	177	157
Molar Flow H2O AR out (mol/h)	0	0	0	131	8	143
Carbon Balance (%)	99.54%	99.57%	99.28%	100.96%	97.61%	107.09%
Methane Conversion to CO2 (%)	59.4%	61.5%	62.2%	61.0%	62.9%	76.5%
Methane Conversion (%)	60.3%	62.4%	63.4%	60.6%	66.0%	70.0%
Oxygen Carrier Utilization (%)	19.9%	22.7%	24.4%	10.3%	21.5%	5.1%
Circulation Rate (kg/h)	139	140	126	192	168	156
Average FR Velocity In (m/s)	0.35	0.36	0.37	0.33	0.36	0.26
Average FR Velocity Out (m/s)	0.41	0.43	0.45	0.37	0.45	0.28
Average FR Velocity (m/s)	0.38	0.39	0.41	0.35	0.40	0.27
Average AR Velocity (m/s)	0.53	0.54	0.55	0.54	0.54	0.54
Riser Gas Velocity (m/s)	9.4	9.6	9.8	9.8	9.6	9.9

Continued on next page…

Table 3. Continued.

	13	14	15	16	17	18
Trial time (min)	68	79	199	95	38	50
Fuel Reactor Temperature (°C)	797	823	807	777	781	759
Air Reactor Temperature (°C)	905	912	921	906	898	900
Fuel Reactor Pressure (kPa)	159	159	159	158	159	159
Inventory (kg)	48	48	46	40	41	35
Gas Residence Time FR (s)	2.16	1.87	1.92	1.23	1.33	1.31
Solids Residence Time FR (s)	708	753	835	1181	704	801
Fuel Reactor Bed Height (m)	0.58	0.57	0.56	0.46	0.47	0.35
Air Reactor Bed Height (m)	0.53	0.54	0.52	0.48	0.49	0.46
Molar Flow CH4 FR in (mol/h)	27.5	108.4	81.9	108.3	35.3	54.0
Molar Flow N2 FR in (mol/h)	520	437	465	621	693	491
Molar Flow CO2 FR out (mol/h)	18	73	53	62	19	28
Molar Flow CO FR out (mol/h)	0	1	0	1	0	0
Molar Flow CH4 FR out (mol/h)	9	31	25	43	16	23
Molar Flow H2 FR out (mol/h)	0	1	1	2	0	1
Molar Flow N2 FR out (mol/h)	513	430	458	614	686	484
Molar Flow H2O FR out (mol/h)	37	155	113	130	39	61
Molar Flow CH4 AR in (mol/h)	1.1	0.3	0.5	0.1	1.0	0.5
Molar Flow Air AR in (mol/h)	1845	1797	1806	1783	1844	1813
Molar Flow CO2 AR out (mol/h)	78	23	35	7	69	39
Molar Flow N2 AR out (mol/h)	1498	1498	1496	1496	1500	1499
Molar Flow O2 AR out (mol/h)	186	184	188	230	213	251
Molar Flow H2O AR out (mol/h)	133	34	58	10	119	64
Carbon Balance (%)	98.05%	96.79%	96.24%	97.73%	98.74%	96.24%
Methane Conversion to CO2 (%)	65.5%	67.6%	64.7%	57.3%	53.8%	52.7%
Methane Conversion (%)	67.8%	71.3%	69.0%	60.1%	55.5%	56.9%
Oxygen Carrier Utilization (%)	4.9%	22.2%	18.2%	35.9%	6.4%	16.3%
Circulation Rate (kg/h)	145	142	126	72	127	79
Average FR Velocity In (m/s)	0.26	0.27	0.27	0.35	0.35	0.25
Average FR Velocity Out (m/s)	0.28	0.34	0.32	0.40	0.36	0.28
Average FR Velocity (m/s)	0.27	0.30	0.29	0.37	0.35	0.27
Average AR Velocity (m/s)	0.54	0.55	0.55	0.55	0.54	0.54
Riser Gas Velocity (m/s)	10.0	9.8	9.9	9.7	9.9	9.8

Continued on next page…

Table 3. Continued.

	19	20	21	22	23
Trial time (min)	33	72	19	56	29
Fuel Reactor Temperature (°C)	776	751	798	814	822
Air Reactor Temperature (°C)	895	899	947	900	956
Fuel Reactor Pressure (kPa)	159	160	161	161	161
Inventory (kg)	37	35	35	36	34
Gas Residence Time FR (s)	1.43	0.98	1.41	1.57	1.13
Solids Residence Time FR (s)	530	382	353	338	294
Fuel Reactor Bed Height (m)	0.38	0.34	0.33	0.34	0.32
Air Reactor Bed Height (m)	0.49	0.50	0.49	0.50	0.48
Molar Flow CH4 FR in (mol/h)	54.1	72.7	173.4	100.1	185.1
Molar Flow N2 FR in (mol/h)	492	657	209	283	283
Molar Flow CO2 FR out (mol/h)	27	25	102	75	121
Molar Flow CO FR out (mol/h)	0	1	1	0	2
Molar Flow CH4 FR out (mol/h)	24	46	46	20	51
Molar Flow H2 FR out (mol/h)	1	2	5	1	11
Molar Flow N2 FR out (mol/h)	484	650	202	276	276
Molar Flow H2O FR out (mol/h)	61	54	255	161	269
Molar Flow CH4 AR in (mol/h)	0.7	0.9	0.0	0.0	0.0
Molar Flow Air AR in (mol/h)	1825	1831	1781	1779	1778
Molar Flow CO2 AR out (mol/h)	50	61	4	1	2
Molar Flow N2 AR out (mol/h)	1499	1495	1499	1497	1496
Molar Flow O2 AR out (mol/h)	235	201	148	196	119
Molar Flow H2O AR out (mol/h)	85	104	0	0	0
Carbon Balance (%)	94.97%	97.59%	86.05%	94.64%	93.75%
Methane Conversion to CO2 (%)	50.5%	33.9%	58.9%	74.6%	65.3%
Methane Conversion (%)	56.0%	37.0%	73.6%	80.2%	72.5%
Oxygen Carrier Utilization (%)	8.8%	6.5%	27.1%	16.8%	25.4%
Circulation Rate (kg/h)	127	156	165	179	194
Average FR Velocity In (m/s)	0.26	0.33	0.18	0.19	0.23
Average FR Velocity Out (m/s)	0.28	0.35	0.29	0.26	0.35
Average FR Velocity (m/s)	0.27	0.34	0.23	0.22	0.29
Average AR Velocity (m/s)	0.54	0.54	0.57	0.54	0.57
Riser Gas Velocity (m/s)	9.8	9.9	10.0	9.6	10.1

Continued on next page…

Table 3. Continued.

	24	25	26
Trial time (min)	29	24	22
Fuel Reactor Temperature (°C)	814	802	783
Air Reactor Temperature (°C)	953	946	932
Fuel Reactor Pressure (kPa)	161	161	160
Inventory (kg)	34	33	31
Gas Residence Time FR (s)	1.12	1.11	1.02
Solids Residence Time FR (s)	313	345	355
Fuel Reactor Bed Height (m)	0.32	0.32	0.28
Air Reactor Bed Height (m)	0.47	0.45	0.44
Molar Flow CH4 FR in (mol/h)	190.8	196.7	202.3
Molar Flow N2 FR in (mol/h)	282	282	282
Molar Flow CO2 FR out (mol/h)	121	118	103
Molar Flow CO FR out (mol/h)	2	3	5
Molar Flow CH4 FR out (mol/h)	56	66	78
Molar Flow H2 FR out (mol/h)	11	17	16
Molar Flow N2 FR out (mol/h)	276	276	276
Molar Flow H2O FR out (mol/h)	269	260	248
Molar Flow CH4 AR in (mol/h)	0.0	0.0	0.0
Molar Flow Air AR in (mol/h)	1779	1779	1778
Molar Flow CO2 AR out (mol/h)	3	4	4
Molar Flow N2 AR out (mol/h)	1496	1496	1496
Molar Flow O2 AR out (mol/h)	106	118	132
Molar Flow H2O AR out (mol/h)	0	0	0
Carbon Balance (%)	94.33%	95.37%	91.83%
Methane Conversion to CO2 (%)	63.6%	59.8%	50.7%
Methane Conversion (%)	70.5%	66.2%	61.3%
Oxygen Carrier Utilization (%)	27.2%	29.0%	32.0%
Circulation Rate (kg/h)	182	171	146
Average FR Velocity In (m/s)	0.23	0.23	0.23
Average FR Velocity Out (m/s)	0.35	0.35	0.34
Average FR Velocity (m/s)	0.29	0.29	0.28
Average AR Velocity (m/s)	0.57	0.56	0.56
Riser Gas Velocity (m/s)	10.0	10.0	9.9